Implementation and Validation of the ISMAR High-Frequency Coastal Radar Network in the Gulf of Manfredonia (Mediterranean Sea)

Lorenzo Paolo Corgnati, Carlo Mantovani, Annalisa Griffa, Maristella Berta, Pierluigi Penna, Paolo Celentano, Lucio Bellomo, Daniel F. Carlson, and Raffaele D'Adamo

***Abstract*—In this paper, a high-frequency (HF) coastal radar network is described, which is established and maintained by the Institute of Marine Sciences (ISMAR) of the National Research Council of Italy (CNR) for the measurement of surface current velocities in the Gulf of Manfredonia, located in the semienclosed Adriatic Sea (Mediterranean Sea), during 2013–2015. The network consisted of four HF radars (HFRs) that provided hourly sea surface velocity data in real-time mode in a netCDF format compliant to the Climate and Forecast Metadata Conventions CF-1.6 and the INSPIRE directive. The hourly netCDF files are disseminated via a Thematic Real-time Environmental Distributed Data Services catalog supporting OGC compliant distributions and protocols for data visualization, metadata interrogation, and data download. HFR velocity data were compared with *in situ* velocity measurements by Global Positioning System tracked surface drifters deployed within the radar footprint. The results show a good agreement, with the root mean square (rms) of the difference between radial velocities from HFR and drifters ranging between 20% and 50% of the drifter velocity rms. The HFR data have also been compared with subsurface velocity profiles from an upward looking acoustic Doppler current profiler (ADCP) during winter 2015, to gain information on the correlation between surface and water column velocities. This information is especially relevant for fishery and coastal management applications, where transport of larvae, sediments, and pollutants in the water column are considered. Results show that, at least in the considered period, the velocity in the water column is well correlated, and there is a good agreement between surface HFR and ADCP data (correlations between 0.95 and 0.75). The Gulf of Manfredonia network has been instrumental to the set up of a core of quality control practices and interoperable data and metadata formats that have been subsequently adopted within the Italian RITMARE network and that are presently discussed and refined at the European level through the projects Jerico-NEXT and INCREASE.**

***Index Terms*—Acoustic Doppler current profiler (ADCP), drifter, high-frequency radar (HFR), interoperability, marine resource, remote sensing, surface current.**

I. Introduction

HIGH-FREQUENCY radars (HFRs) are well established and widely used instruments for measuring surface currents and wave parameters [1], providing effective coverage of large coastal ocean areas. Coastal regions are especially vulnerable and exposed to human activities, such as ship traffic, port activities, border security, and resource exploitation. HFRs play an important role in monitoring transport and dispersion processes, which are crucial for protecting marine biodiversity and mitigating anthropogenic hazards.

An HFR uses ground wave propagation and the relationship between the transmitted signal (in the high-frequency range 3–30 MHz, with corresponding wavelengths in the range 100–10 m) and the signal backscattered by surface ocean waves with half the transmitted wavelength, referred as the Bragg scattering [2].

Through the analysis of the Bragg peaks in the backscattered signal, it is possible to obtain the information of the seawater velocity [3]. These peaks are generated by the coherent summation of the signals backscattered by surface gravity waves with half the wavelength of the emitted signal and moving in a radial path either away from or toward the radar. The backscattered signal is Doppler shifted depending on the speed of the scattering surface. In the absence of surface currents, the total shift will only be that due to the surface gravity wave propagation. The shift due to the phase speed of surface waves can be separated from the total frequency shift, thus the shift due to surface current components in the direction of the antenna can be isolated. From the frequency shift in the first-order backscatter, the surface current velocity is retrieved, whereas from both the first-

Manuscript received May 23, 2017; revised December 20, 2017; accepted March 29, 2018. Date of publication May 10, 2018; date of current version April 12, 2019. This work was presented in part at the MTS/IEEE OCEANS Conference, Genova, Italy, May 18–21, 2015. *(Corresponding author: Lorenzo Paolo Corgnati.)*

Associate Editor: E. Gill.

L. P. Corgnati, C. Mantovani, A. Griffa, and M. Berta are with the Institute of Marine Sciences (ISMAR), National Research Council (CNR), La Spezia 19032, Italy (e-mail: lorenzo.corgnati@sp.ismar.cnr.it; carlo.mantovani@cnr.it; annalisa.griffa@sp.ismar.cnr.it; maristella.berta@sp.ismar.cnr.it).

P. Penna is with the Institute of Marine Sciences (ISMAR), National Research Council (CNR), Ancona 60125, Italy (e-mail: pierluigi.penna@an.ismar.cnr.it).

P. Celentano was with the Dipartimento di Scienze e Tecnologie, Universitá degli Studi di Napoli "Parthenope," CoNISMa, Napoli, Italy. He is now with the Institute of Marine Sciences (ISMAR), National Research Council (CNR), La Spezia 19032, Italy (e-mail: paolo.celentano@sp.ismar.cnr.it).

L. Bellomo was with MIO, Université du Sud Toulon-Var, Aix-Marseille Université, CNRS/INSU, IRD, UM 110, La Garde 83130, France (e-mail: lucio.bellomo@univ-tln.fr).

D. F. Carlson was with the Institute of Marine Sciences (ISMAR), National Research Council (CNR), La Spezia 19032, Italy. He is now with the Department of Earth, Ocean, and Atmospheric Sciences, Florida State University, Tallahassee FL 32306 USA and also with the Arctic Research Centre, Aarhus University, Aarhus DK-8000, Denmark (e-mail: danfcarlson@bios.au.dk).

R. D'Adamo is with the Institute of Marine Sciences (ISMAR), National Research Council (CNR), Lesina 71010, Italy (e-mail: raffaele.dadamo@fg.ismar.cnr.it).

Digital Object Identifier 10.1109/JOE.2018.2822518

0364-9059 © 2018 IEEE. Translations and content mining are permitted for academic research only. Personal use is also permitted, but republication/redistribution requires IEEE permission. See http://www.ieee.org/publications_standards/publications/rights/index.html for more information.

order and the second-order backscatter, the wave parameters are evaluated [4].

HFRs provide continuous information in terms of 2-D surface velocity. Each HFR node generates maps of the velocity radial components over a range of 30–200 km from the coast, with typical spatial resolution of 1–6 km, angular resolution of 5° [5], [6], and integration time of 0.25–1 h [7]. The spatial horizontal averaging in range and azimuth depends on the radar configuration, whereas the exponentially weighted vertical averaging occurs from the surface to a depth of $\lambda/8\pi$, where λ is the transmitted wavelength [8], which corresponds to values in the range 0.4–4 m, for the considered transmitting frequencies.

Since the Doppler shift only resolves the current components moving along radial directions (toward or away) with respect to the antenna, total surface velocity maps can be obtained by geometrically combining data from at least two radar sites in their overlapping coverage, provided some geometrical constraints are satisfied.

The main uncertainty source in the combination of radials into total velocities is the geometry of the radar network (i.e., reciprocal positions of the contributing sites). The geometric uncertainty is based on the incidence angles between the radial component vectors at the grid point of the total vector map, commonly referred as the geometric dilution of precision (GDOP) [9]. The more the relative angles between radials move away from orthogonality, the higher is the geometric uncertainty. The accuracy of the radial-to-vector mapping also depends on the number of radial velocities from each radar site involved in the combination process, known as the geometrical dilution of statistical accuracy [10].

Other unavoidable error sources affecting radial data are related to electromagnetic interferences [11], ionosphere clutter, or other environmental noise [12] and antenna pattern distortion for signal processing methods that require antenna pattern measurement (APM), i.e., direction finding [13]. The first two factors result in a decreased signal-to-noise ratio (SNR), whereas the third factor introduces errors in the received signal phase and amplitude. SNR variations cause variability in time and space of the available radial data coverage. Measuring the antenna pattern and using it in the signal processing allow in most of the cases for removing biases caused by the pattern distortions [13].

Many interpolation techniques have been developed to fill the gaps caused by the aforementioned issues, based on a 2-D variational approach [14], an open-boundary modal analysis [15], normal modes [16], statistical mapping [17], [18], penalized least square regression [19], and weighting based on the decorrelation scale [20].

HFRs have greatly improved the ability to study transport in coastal areas. In the past, the possibilities were limited to pointlike current meter measurements that were used to create progressive vector diagrams (PVDs) [21]. However, PVDs assume that the current meter measurements are representative of conditions near the observation location. This assumption is often false in the coastal zone, where variability of ocean currents is high due to changes in bathymetry, freshwater inflows, wind forcing, etc.

HFRs are widely used in coastal area applications, in particular, to provide information on ocean current transport for monitoring and predicting the spreading of pollutants and biological quantities [22], and for search and rescue activities [17], [23]. Transport is typically quantified by computing pseudo-Lagrangian trajectories of virtual particles [24]. From the numerical modeling perspective, HFR data offer great benefits, as they cover significant portions of coastal ocean model domains and can be used for blending [25] and assimilation [26], [27] tasks.

To provide a high level of reliability for all these applications, HFR data need to be validated using appropriate *in situ* data. As for most remote sensing measurements, validation is not a straightforward task [28], [29] because the characteristics of *in situ* and remote data are often different.

Since HFRs produce velocity data at the ocean surface, the most suitable *in situ* data for comparison are provided by Lagrangian surface floating buoys (drifters) that typically give velocity information in the first meter from the surface [30]. It should be noted that there is a mismatch in the horizontal resolution since drifters measure velocities at the scale of their physical size, of the order of 1 m, while HFR data are averaged over cells with typical size of the order of 1–3 km^2 [31]. For this reason, velocities from the two platforms are not expected to coincide, and their typical differences are expected to be of the order of the environmental variability within the cell.

Another important issue, especially for applications regarding transport of ecological quantities that are not restricted to the very surface, is how to complement HFR data with other *in situ* data that provide information on interior velocity and stratifications. Acoustic doppler current profilers (ADCPs) are especially well suited for that [32], [33], even though they suffer from the same problem as the drifters, i.e., their information is typically pointlike in the horizontal with respect to the cell averaged radar information.

In this paper, we present the HFR network implemented by the Institute of Marine Sciences (ISMAR) of the National Research Council of Italy (CNR) in the Adriatic Sea (Mediterranean Sea) to measure surface currents in the relevant ecological area of the Gulf of Manfredonia. The gulf is a well-known nursery area for small pelagic fishes, and the deployment of the HFR network has been motivated by the study of larval transport to contribute to the improvement of sustainable fishery management of sardines [34]. The paper focuses on the following three main aspects.

1) The network architecture is presented, detailing its infrastructural core, system performance, and processing methods and reviewing recent developments in interoperability.
2) The comparison of the HFR velocity data with surface drifters' data and the effects of antenna pattern distortion are discussed.
3) The HFR surface velocity information are complemented with the information on velocity profiles in the water column from ADCP during a winter period (corresponding to sardine spawning period).

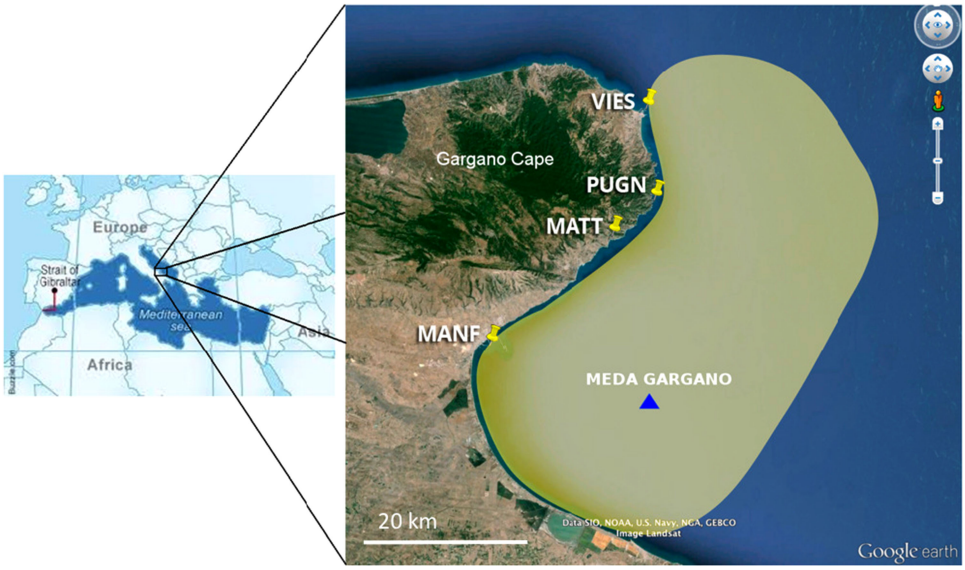

Fig. 1. Map of the ISMAR HFR network node locations in the Gulf of Manfredonia, Southern Adriatic Sea. The highlighted area indicates the typical coverage of the radar network. The blue triangle indicates the position of the seamark Meda Gargano.

This paper is organized as follows. Section II describes the ISMAR HFR network and the interoperability framework of data production. Section III presents the results of the comparison carried out with surface drifters to assess the network operational regime. Section IV explains the analysis of correlation between HFR surface currents and currents in the water column. Finally, in Section V, summary and conclusions are provided and future developments of the network are discussed.

II. High-Frequency Radar network

The ISMAR HFR network has been run operationally during the period 2013–2015 to monitor surface currents in the Gulf of Manfredonia [35], as shown in Fig. 1.

The Gulf of Manfredonia is situated south of the Gargano Promontory (see Fig. 1) along the western (Italian) coast of the Adriatic Sea, a subbasin of the Mediterranean Sea. The Gulf has an approximate diameter of ≈30 km and shallow depths of less than 20 m. The circulation in the Adriatic Sea is generally cyclonic, with a swift boundary current flowing southward along the western boundary called the Western Adriatic Current (WAC) [36], [37]. The WAC typically detaches from the coast at the Gargano Cape and reattaches with the south of the Gulf [38], [39]. This general pattern is modulated depending on the seasons and the winds [40]. Fig. 11 of [38] represents the circulation in the studied area, based on average velocities from historical drifters. Northwesterly winds are downwelling prone and tend to increase the strength of the WAC moving it closer to the coast, whereas southeasterly winds are upwelling prone and tend to weaken the WAC, moving it offshore and occasionally reversing it. The circulation in the Gulf is influenced by the large-scale WAC behavior and also by a number of more local forcings, such as wind and river inflow [41]. Mesoscale and submesoscale recirculations, both cyclonic and anticyclonic, are often observed within the Gulf. Examples of velocity patterns measured by the HFR are shown in Fig. 2, and will be further discussed in Section III.

The network has been designed and developed within the Co.Co.Net (www.coconet-fp7.eu) and SSD-Pesca (www.cnr.it/sitocnr/IlCNR/SeiProgettiPerIlSud/p3.html) projects with the aim of contributing to the study of connectivity and transport of fish larvae in the Adriatic Sea, and the data analysis was carried out also within the JERICO-NEXT (www.jerico-ri.eu) project.

The network has also been funded by the Italian flagship project RITMARE (www.ritmare.it), which is focused on the integration of local observing systems into a unified operational Italian framework and on the harmonization of data collection and management procedures, fostering interoperability among data providers. The Gulf of Manfredonia's installation has been instrumental to the set up of a core of quality control (QC) practices and interoperable formats that have been subsequently used within the RITMARE network [42], and that are presently discussed and refined at the European level through the projects JERICO-NEXT and INCREASE [43].

The ISMAR HFR network is comprised of four radar systems, and it has been implemented and operated through the joint efforts of the two ISMAR laboratories of La Spezia and Lesina, Italy. The four sites were located along the Gargano coast and they have been selected, given some constraints by the shape of the coastline and the existence of the necessary infrastructures, with the best available spacing and geometry, to have a satisfactory coverage of the area of interest. The HFR network coverage spanned an area of approximately 1700 km^2. The four nodes of the network were situated in Vieste (site code VIES) near the lighthouse on the S. Eufemia island, at the lighthouse Torre Preposti in Pugnochiuso (site code PUGN), on the coast of Mattinatella (site code MATT), and on top of the green beacon of the port of Manfredonia (site code MANF). To have an optimal coverage, the theoretical distance between two adjacent sites operating at 25 MHz should be around 20 km, but in fact, it depends on the coastline shape and on the presence and accessibility of some basic infrastructures. The linear distance between VIES and PUGN sites is 12 km, the linear dis-

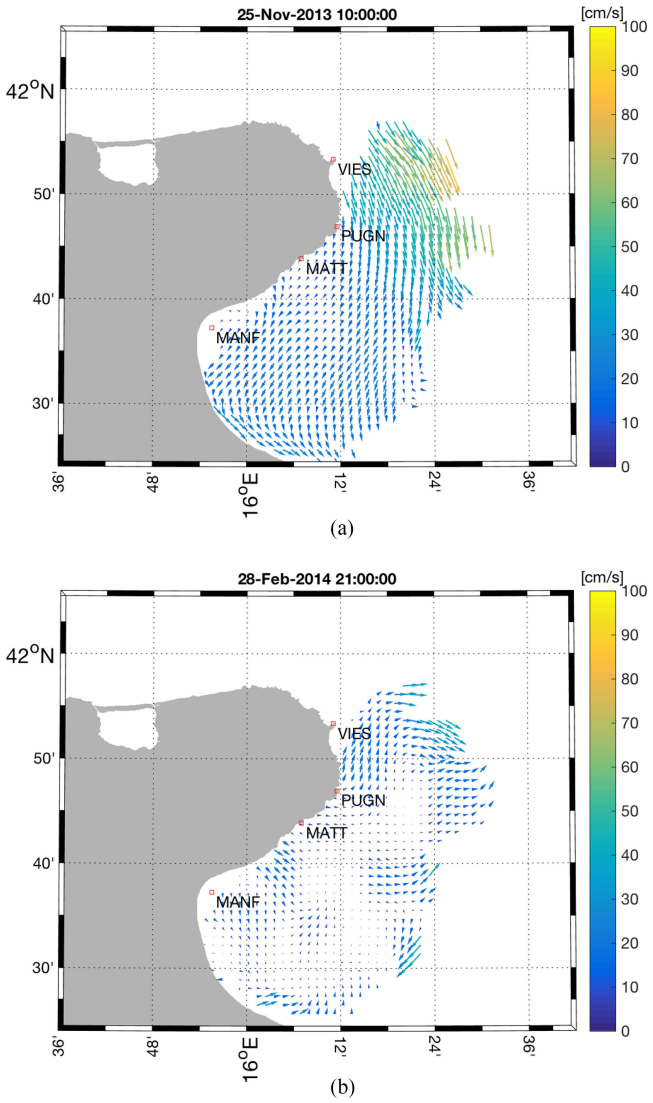

Fig. 2. Two examples of surface water current maps in the Gulf of Manfredonia as measured by the ISMAR HFR network. (a) Current map recorded during the November 2013 experiment is reported: as it happened for the whole experiment period, the currents are dominated by a large-scale pattern. (b) Current map recorded during the February 2014 experiment is reported: as for the whole experiment period, many different small-scale recirculations are visible inside the Gulf of Manfredonia.

tance between PUGN and MATT sites is 8.5 km, and the linear distance between MATT and MANF sites is 20 km. The first two distances were chosen smaller than the ideal one because of the considerable convexity of the coast between MATT and VIES sites. Table I lists the geographic coordinates of the four installations, whereas Fig. 3 shows the radar installations.

The network architecture is made up of three operational layers. The ground layer consists of the infrastructural components, the acquisition instruments, and the data management and storage modules. The processing layer is responsible for the data processing, in particular QC, radial data combination into total vectors, data storage, and data dissemination. The publishing layer visualizes the total velocity maps and distributes the data, both radial and total velocities, in different interoperable formats. In the following, the detailed description of the three layers is provided.

A. Ground Layer

The ISMAR network is composed of four SeaSonde direction finding systems manufactured by Codar Ocean Sensors, Mountain View, CA, USA [44]. All the devices operate in the high-resolution frequency band of 25 MHz.

Each SeaSonde HFR station is equipped with co-located receiving and transmitting antennas. The antennas are connected to the radar transmit device and receive device, which are controlled by a desktop computer. The transmitting antenna is omnidirectional and the receiving antenna consists of three co-located antenna elements, two oriented on the horizontal plane (antenna loop 1 along the x-axis and antenna loop 2 on the y-axis) and one on the vertical plane (monopole along the z-axis). The system is thus able to receive returning signals over all 360° and to resolve up to two signals coming from two different directions for each Doppler spectral frequency, either for positive and negative shifts.

The radars process time series (receive antenna voltage versus time) of the received sea echoes to retrieve the current velocity data. The velocity resolution is determined by the operating frequency and by the sampling time, i.e., the duration of each time series. For a default 25-MHz SeaSonde configuration, which has been adopted for the presented systems, it corresponds to ∼0.02 m/s.

The bearing angle of the velocities is determined through the comparison between phases and amplitudes of data collected from the co-located directional elements in the receiving antenna at each spectral point (i.e., range and frequency). This process is operated by the direction finding algorithm multiple signal classification (MUSIC) [45]–[47], which is optimized and patented for SeaSonde instruments. At the end of the signal processing, hourly maps of surface current radial velocity are available in polar coordinates. Table I summarizes the configuration parameters of the four nodes of the Gulf of Manfredonia network, as described in [35].

Since the calculation of the velocities' bearing for direction finding HFR systems depends on the actual beam pattern of the receive antenna [12], antenna patterns have been measured for each radar system (antenna calibration procedure). In this way, when distortion is acceptable, the processing pipeline takes into account possible pattern distortions due to the antenna surroundings and therefore radial data can be considered more reliable, because biases due to pattern distortions can be removed.

Since the monopole is omnidirectional, its theoretical pattern is a circle of constant radius around the antenna post, whereas the theoretical (ideal) pattern of the cross loops has a peak in loop 1 that coincides with the null of loop 2 and *vice versa*, and the look direction of the whole system lies in one null of the loop 1 pattern.

For all the radar sites, antenna patterns have been measured from a boat using a transponder. After having synchronized the SeaSonde computer clock with the boat Global Positioning

TABLE I
GEOGRAPHIC COORDINATES AND OPERATIONAL SETTINGS OF THE ISMAR HFR NETWORK NODES DEPLOYED IN THE GULF OF MANFREDONIA

Site Code	VIES	PUGN	MATT	MANF
Site Location	Vieste	Pugnochiuso	Mattinatella	Manfredonia
Latitude	$41°53'19.87"N$	$41°46'57.24"N$	$41°43'51.96"N$	$41°37'14.41"N$
Longitude	$16°11'5.49"E$	$16°11'31.86"E$	$16°6'58.32"E$	$15°55'30.95"E$
Transmit Frequency [MHz]	24.525	26.275	26.275	26.275
Bandwidth [kHz]	150	150	150	150
Spatial Resolution [km]	1	1	1	1
Angular Resolution [deg]	5	5	5	5
Range Cut-off [km]	44	44	44	44
Sweep Rate [Hz]	2	2	2	2
Doppler Resolution [Hz]	0.5	0.5	0.5	0.5
Transmit Power [W]	33	38	44	35

Fig. 3. ISMAR HFR network installations in the Gulf of Manfredonia. From left to right: MANF, PUGN, MATT, and VIES.

System (GPS) clock, the boat has been moved at constant speed along a circular arc of radius 1 km, centered on the receive antenna. The boat GPS logged the tracks and the SeaSonde systems logged the received signal time series.

From the GPS tracks and the HFR time series, the antenna patterns have been computed using the Codar Cross Loop Patterner application. No filtering has been applied to the data used to compute the patterns. To maintain the angular resolution of the receive antennas, i.e., 5°, reduction and interpolation parameters have been both set to 5°. In this way, no effective interpolation took place. The resulting antenna patterns have been smoothed at 5°. It has to be noted that a reduction operator causes all bearings within +/− half the reduction parameter to be averaged into one point. The smoothing operator averages bearings over +/− half the smoothing parameter. It does not reduce the number of points like the reduction operator does.

Fig. 4 shows the measured antenna patterns for each radar site and highlights the good health of both monopole [see Fig. 4(a)] and cross-loop patterns [see Fig. 4(b)] for all the sites. In particular, in Fig. 4(b), it is evident that all the cross-loop patterns, besides the unavoidable distortions due to the surrounding environment, fulfill the constraints of the theoretical conditions. The cross-loop pattern of the MANF site turns out to be the closest to the ideal shape (i.e., the less distorted). On the other hand, the monopole and cross-loop patterns of the VIES site contain some distortions, which could be considered intrinsics in the antenna since the installation area was clear from metal structures and obstacles and no interfering environmental factors were recorded during the operational period. Furthermore, the APM procedure has been repeated multiple times for all the sites in the operational period and no differences were recorded in the patterns measured in different times.

At each installation, all produced data (diagnostics, log, configurations, spectra, and radial velocities) are locally stored and automatically synced to the central network attached storage (NAS), referred as the RADARDISK SP and located in the ISMAR lab, La Spezia, Italy.

Each site is equipped with a communication module based on a GPRS/Universal Mobile Telecommunications System (UMTS) modem with high-gain omnidirectional external antenna, providing the bandwidth necessary to perform remote management (diagnostic checks and reprogramming tasks), radial velocity data transfer, and main data backup to the RADARDISK SP. Periodic manual data backup is needed for full data copy.

The temperature and humidity conditions of the control rooms hosting the radar devices are maintained by air-conditioning systems and the electrical safety of the instrumentation is guaranteed by an uninterruptible power supply, providing voltage

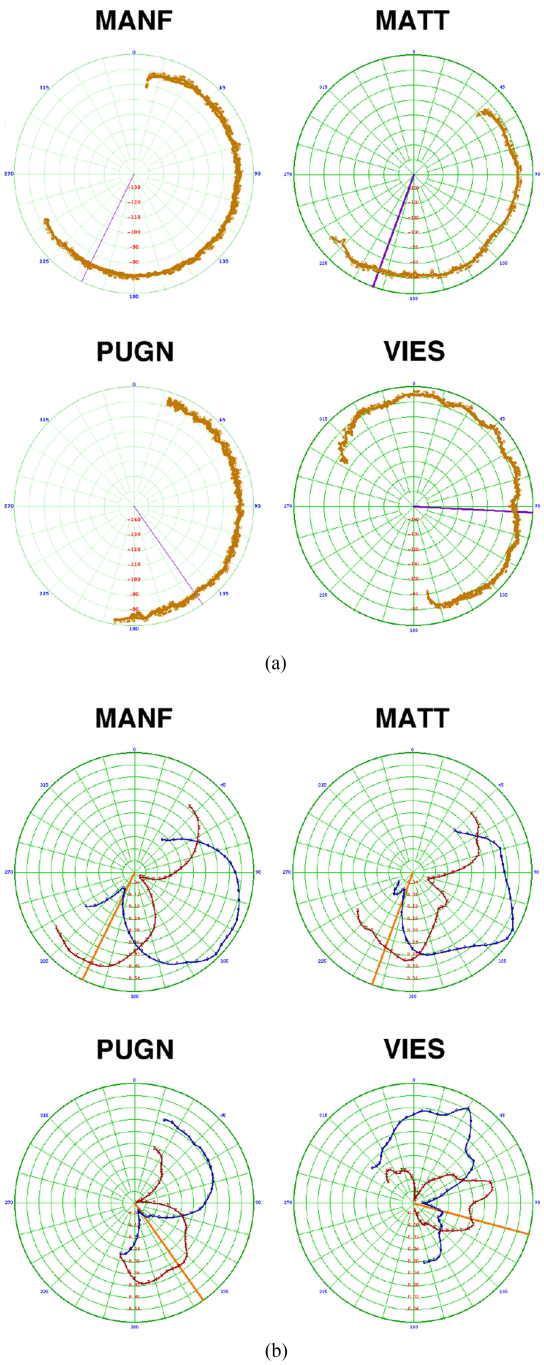

Fig. 4. Antenna patterns measured at each site of the ISMAR HFR network in the Gulf of Manfredonia. (a) Monopole patterns measured at each site of the ISMAR HF radar network in the Gulf of Manfredonia. (b) Cross-loop patterns measured at each site of the ISMAR HF radar network in the Gulf of Manfredonia

stability and a short-emergency power to all the loads when the main power fails.

Operating with the presented setup, the ISMAR HFR network in the Gulf of Manfredonia guaranteed high-level performances, in terms of temporal and spatial coverage, optimal geometrical configuration (necessary for radial combination into total vectors), SNR, and noise floor (NF).

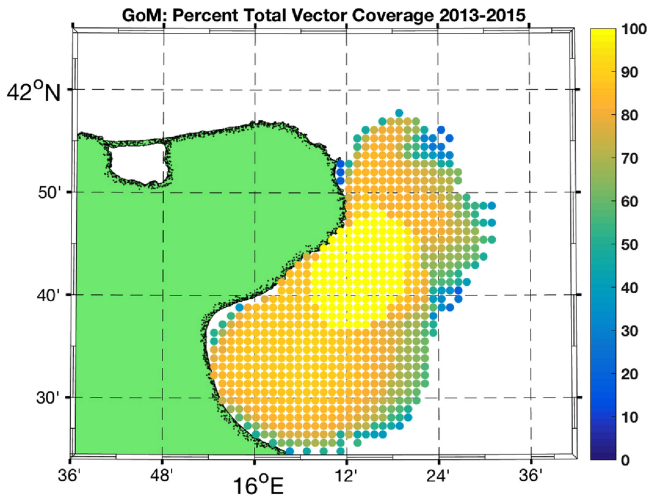

Fig. 5. Percentage of time with which total velocities have been produced on the spatial coverage along the total operational period of the network (August 2013 to June 2015).

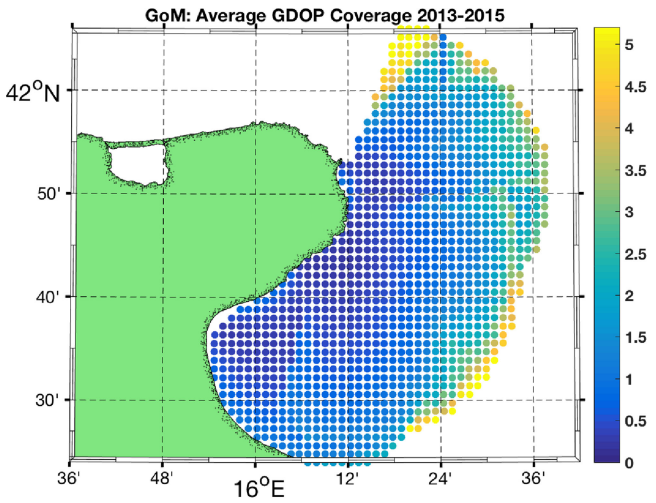

Fig. 6. Average GDOP on the spatial grid along the total operational period of the network (August 2013 to June 2015).

Fig. 5 shows the percentage of time with which total velocities have been produced on the spatial coverage along the total operational period of the network (August 2013 to June 2015). 62.42% of the spatial coverage have been producing data more than 80% of the operational time. This is a satisfactory performance, considering that the ISMAR HFR network was not producing data for security or safety services and infrastructural works at the lighthouses of Manfredonia and Vieste required to turn off the radar devices for more than two months.

The planned geographical configuration of the radar network proved to be robust, as depicted in Fig. 6. In fact, the average GDOP on the spatial grid along the network operational period ranged in 0.1650–10.4028, with 76.89% of the total network spatial coverage taking GDOP values lower than the threshold used for the GDOP-based QC, i.e., $\sqrt{2}$. It has to be noted that the GDOP to be compared against the GDOP QC threshold is evaluated for each total file.

TABLE II
AVERAGE SSN AND NF FOR ALL THE SITES AND ALL THE ANTENNA ELEMENTS ALONG THE OPERATIONAL PERIOD OF THE ISMAR HFR NETWORK DEPLOYED IN THE GULF OF MANFREDONIA (AUGUST 2013 TO JUNE 2015)

Site Code	VIES	PUGN	MATT	MANF
SSN Loop 1 [dB]	33.9203	35.2741	39.5168	32.7739
SSN Loop 2 [dB]	34.8475	33.6016	38.5380	36.9787
SSN Monopole [dB]	39.8443	35.2221	41.2408	34.4831
NF Loop 1 [dBm]	-144.3589	-140.9079	-143.1999	-144.1704
NF Loop 2 [dBm]	-141.3720	-139.6374	-140.3659	-139.9063
NF Monopole [dBm]	-131.3930	-131.6818	-130.9804	-131.2792

On the hardware system performance side, along all the operational period of the network, the four stations kept satisfactory levels of mean SeaSonde cross spectra signal-to-noise (SSN), a parameter evaluated by Codar SeaSonde software and related to SNR, and of mean NF. In particular, the SSN of loop 1, loop 2, and monopole are calculated by the SeaSonde software by finding a peak signal at a single range cell on just the monopole and taking the difference from the signal level to the NF for each antenna element. The NF of loop 1, loop 2, and monopole are evaluated by the SeaSonde software by averaging the noise levels in each range cell. The values recorded in the radial files are for the range cell with the maximum SSN.

The mean SSN ranged in [32.7739, 39.5168] dB for antennas' loop 1, [33.6016, 38.5380] dB for antennas' loop 2, and [34.4831, 41.2408] dB for the monopoles. The mean NF ranged in [−144.3589, −140.9079] dBm for antennas' loop 1, [−141.3720, −139.6374] dBm for antennas' loop 2, and [−131.6818, − 130.9804] dBm for the monopoles. Table II reports the average SSN and NF for all the sites and all the antenna elements along the operational period of the network, whereas Fig. 7 shows the time series of SSN and NF for all the sites and all the antenna elements along the operational period of the network.

In particular, Fig. 7 highlights the good SSN dynamic and the constant level of NF at the sites of MATT and PUGN. At the MANF site, the SSN dynamic was also good, but it presented some time variations, probably due to human activities, since the antenna was located within the city area (whereas MATT and PUGN sites were located in rural and isolated areas). The NF was constant but presented some peaks, probably due to the same reason. The time history of the SSN dynamic and the NF level at the VIES site is more complex. Starting from January 2014, a worsening in the antenna performance was observed: a significant noise level increase in the monopole channel was recorded, while it remained almost stable on the loop 1 channel and increased a little on loop 2 channel. As suggested by the manufacturer, some tests were performed to analyze the graphs of transmitted and reflected power readings, but it came out that these were stable and within the normal operational values. This indicated that the problem was not likely to be related to the antenna or the wiring between the receiver and the antenna, but to the electronics modules. As a consequence, the blanking board located in the transmitter chassis was replaced in June 2014, and in July 2014, the system went back to normal functioning until the end of the operations in June 2015. Despite these problems, no critical reduction in coverage was recorded in the period January 2014 to June 2014.

B. Processing Layer

The core of the processing layer consists of the central calculation server RADARCOMBINE SP and the RADARDISK SP NAS, both located in the ISMAR lab, La Spezia, Italy.

The RADARCOMBINE SP server runs the AutoPuglia software tool responsible for the automatic real-time data processing, storage, and dissemination. AutoPuglia operates the real-time collection of the hourly radial data, the organization in working data structures, the QC processing, the radial combination of total vectors, the data distribution, and the data storage. The tool has been developed by the radar research group of the ISMAR Institute, La Spezia, Italy, based on MATLAB routines, as it uses the open source libraries HFR_Progs 2.1 (cencalarchive.org/∼cocmpmb/COCMP-wiki/index.php/MainPage) [48] and M_Map (https://www.eoas.ubc.ca/∼rich/private/mapug.html) [49], which are suited for MATLAB environment.

As detailed in [35], AutoPuglia automatically accesses the folder on RADARDISK SP where radial data are synced from all the network nodes, organizes them into a proper data structure, and processes them.

A scheme of flags indicating whether some of the expected files are missing or if the processing of the data is complete or corrupted allows AutoPuglia to avoid closing the data processing of a given timestamp if some tasks went wrong.

For the Gulf of Manfredonia network, AutoPuglia performs the combination of radial velocities into total velocity vectors on a geographic latitude/longitude grid in the area 15.6°–16.7°E and 41.4°–42.1°N, with spatial resolution equal to 1.5 km and a transverse Mercator projection.

The combination of radial vectors into total vectors is performed using the unweighted least squares fitting (UWLS) algorithm. The UWLS approach [50]–[52] assumes that, for each grid point, the radial velocities within the search radius are produced by a uniform velocity vector, i.e., the correlation of the current vector is assumed to be one everywhere within the search radius and zero outside. The search radius used by the AutoPuglia software for the Gulf of Manfredonia is 3 km. No gap filling procedure is applied to total data.

Before combination, radial velocities are processed for QC by applying a velocity threshold and a mask identifying velocity vectors on land. The velocity threshold was set to 1.2 m/s according to the typical current value of the investigated area and has been kept static for all produced radial vectors.

The QC procedures applied to total velocities are a velocity threshold and a GDOP threshold. The velocity threshold applied to total vectors was set to 1.2 m/s and was kept static for all produced total vectors. The GDOP in HFR measurements is more localized and time-dependent due to the sparse solutions of the MUSIC algorithm compared to the GDOP in satellite remote sensing [20]. Thus, since for HFR measures, the GDOP depends

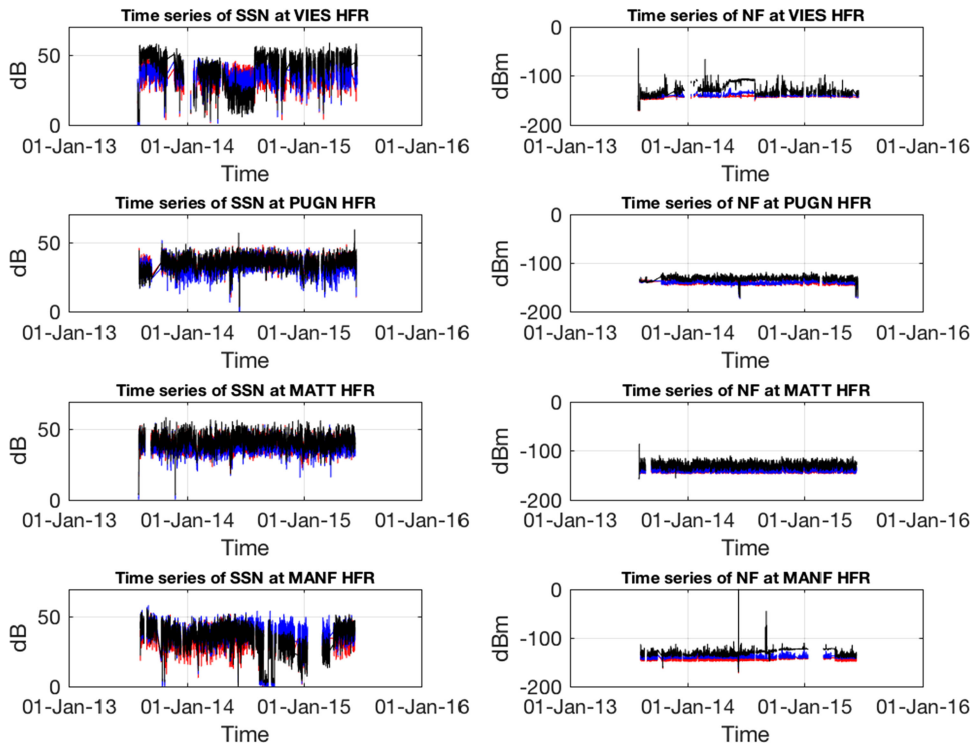

Fig. 7. Time series of SSN and NF for all the sites and all the antenna elements along the operational period of the ISMAR HFR network deployed in the Gulf of Manfredonia (August 2013 to June 2015).

on the number of available radial velocities within the search radius and their bearing angle, GDOP values to be compared against the QC threshold were evaluated for each grid cell for each combination time (i.e., hourly) based on radials contributed from each site. The GDOP threshold was set to $\sqrt{2}$, thus meaning that radial velocities are combined into total velocities only if their incidence angles lie in the range $45^\circ - 135^\circ$. The GDOP threshold has been kept static for all produced total vectors.

The outputs of AutoPuglia tool are radial and the total velocity data are in graphical and netCDF format. Fig. 2 shows examples of total velocity maps, whereas Fig. 8 shows examples of radial velocity maps.

As part of the activities was carried out within the EuroGOOS HFR Task Team, Jerico-Next, INCREASE, and RITMARE projects, the design and implementation of a standard interoperable format for HFR data and metadata have been performed and tested in the framework of the Gulf of Manfredonia network.

The netCDF file structures have been defined for radial and total data according to the standards of Open Geospatial Consortium (OGC) [53] for the access and delivery of geospatial data. Its metadata scheme complies with the Climate and Forecast (CF) Metadata Conventions CF-1.6 [54] and the INSPIRE directive [55], and fulfills the recommendations given by the U.S. Radiowave Operators Working Group (US ROWG) [1], [56].

The netCDF structures contain the current variable fields (eastward and northward seawater velocity, surface seawater velocity, and radial seawater velocity), the error fields (surface eastward and northward seawater velocity standard deviation (std), surface seawater velocity std, covariance of surface seawater velocity, and geometrical dilution of precision), the QC flags and all metadata related to site installations, sensors specifications, operational settings, geospatial information, and dissemination policy.

All the variable names and the attribute names are terms of controlled vocabularies, namely CF-1.6 standard names, GCMD Science Keywords [57], and SeaDataNet P09 (http://vocab.nerc.ac.uk/collection/P09/current/) [58], to enforce the semantic interpretation of the data structure.

The generated radial and total velocity files are then automatically stored and disseminated.

C. Publishing Layer

The publishing layer automatically sends the generated netCDF files of radial and total velocity data to a Thematic Real-time Environmental Distributed Data Services (THREDDS) server [59] responsible for data distribution. In particular, the netCDF files are attached in real-time mode to a THREDDS catalog that provides metadata and data access.

The catalog offers different remote-data-access protocols [59], such as open source project for a network data access protocol, Web coverage service, Web map service (OGC standards), as well as pure HTTP or NetCDF-Subsetter. These protocols allow for metadata interrogation and data download (even subsetting the data set in terms of time and space) while embedded clients, such as GODIVA2, NetCDF-JavaToolsUI, and Integrated Data Viewer, grant real-time data visualization directly via browser and allow for interactively navigating within the plotted maps, saving images, exporting–importing

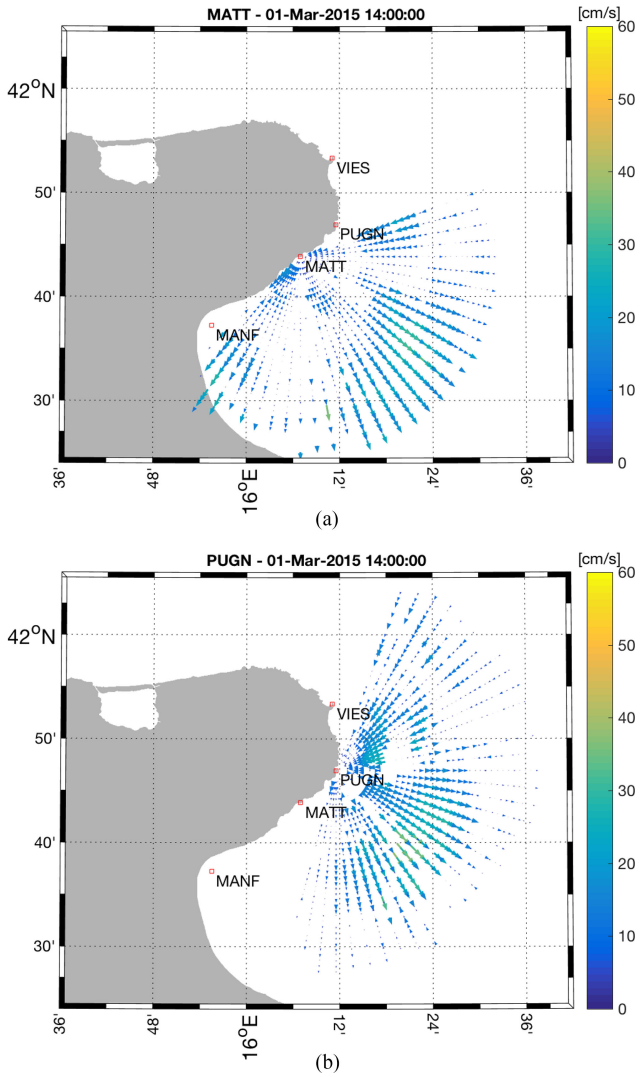

Fig. 8. Examples of radial velocity maps measured by the ISMAR HFR network in the Gulf of Manfredonia. (a) Radial velocity map measured at the MATT site. (b) Radial velocity map measured at the PUGN site.

on Google Earth, and generating animations in selected time intervals.

Data on THREDDS catalog are accessible both in aggregated and in nonaggregated configuration.

The access to data is free and it is licensed under a Creative Commons Attribution 4.0 International License.

The ISMAR HFR network catalog is currently managed by the Institute of Atmospheric Sciences and Climate of the National Research Council of Italy (CNR-ISAC) and is available at http://ritmare.artov.isac.cnr.it/thredds/ritmare/CoastalRadarOS/HF_RADAR/Gulf_of_Manfredonia/catalog.html.

The RITMARE website (http://www.ritmare.it/articolazione/sottoprogetto-5/sp5-wp2/sp5-wp2-azione3) presents the ISMAR HFR network and gives access to the surface water current maps and data files through a link to the THREDDS catalog.

III. Comparison With Surface Drifters

As mentioned in Section I, HFR velocities are obtained vertically averaging within a surface layer that extends from the surface to a depth of $\lambda/8\pi$, where λ is the transmitted wavelength [8]. At the operational center frequency of the ISMAR HFR network, i.e., 25 MHz, the transmitted wavelength is 12 m, so that the averaging layer is 0–0.48 .

To assess the accuracy of the current measured by the HFRs, the radar velocities have been compared with the velocities measured by surface drifters deployed within the network coverage. Drifters [30] are Lagrangian instruments that follow the surface current with good approximation and provide direct information on horizontal velocity and transport. CODE-based drifters [30], [60] have been chosen as the most suitable platforms for the comparison experiments since they are drogued in the first meter below the surface. CODE drifters are designed to minimize slippage due to the direct action of wind and waves [61], and they follow the currents with small errors, typically within 0.01–0.03 m/s [61].

Even though HFR and CODE drifters are basically compatible regarding vertical sampling, it should be noted that there are some quantitative differences between the two instruments since drifters provide a bulk average over the first meter, whereas HFRs provide exponentially weighted averages over $\approx$0.5 m (for a central operating frequency of 25 MHz). These differences can play a role in the presence of very strong shears in the upper ocean.

In the horizontal direction, on the other hand, a clear mismatch of scales is expected since HFR based velocity is averaged over the 2-D grid cell with a size of 1.5 km, whereas drifter velocity is averaged over the scale of the instrument, i.e., $\approx$1-m scale. As a consequence, the comparison between HFR and drifters can be considered satisfactory when it falls in the range of expected variability within the horizontal grid [31]. Results from the literature suggest that velocity differences of the order of 0.05–0.15 m/s can be considered acceptable and within the expected variability at the HFR subgrid scale [9], [29], [31], [62]–[70].

All the drifters used in the experiments were equipped with GPS receivers gathering position data every 15 min with an accuracy of approximately 5–10 m. Drifter positions were processed to remove outliers and spikes [71], [72] and interpolated at uniform 1-h intervals [73]. Their velocities along trajectories were computed from the positions by central finite differences.

Two comparison experiments have been carried out, one in November 2013 and one in February 2014.

In November 2013, seven drifters were launched within the radar coverage region, six of which in triplets [74] released with nominal initial distance of approximately 100 m (see Fig. 9).

The experiment was supposed to consist of multiple sets of catch-and-release exercises, but because of the rough weather, only one release was performed and the drifters were retrieved after a few hours (less than 12 h). The sum of the time spent by all the drifters within each radar coverage t_d ranges between approximately 40 and 70 h, depending on the individual radar (see Table III).

In February 2014, five drifters were launched within the radar coverage and let free to drift (see Fig. 12). Before the launches, a preliminary study was performed based on historical HFR current data, to identify the best release locations to maximize

TABLE III
RESULTS OF THE SURFACE LAYER VALIDATION EXPERIMENTS OF NOVEMBER 2013 AND FEBRUARY 2014

Site code	t_d [hours]		rms_d^R [m/s]		$rmse$ [m/s]		μ [m/s]		ρ_0^2	
	Nov	Feb	Nov	Feb	Nov	Feb	Nov	Feb	Nov	Feb
VIES	43	87	0.19	0.15	0.04 (0.17)	0.08 (0.12)	0 (0.01)	0 (-0.01)	0.93 (-0.13)	0.91 (0.65)
PUGN	45	400	0.22	0.12	0.07 (0.09)	0.07 (0.09)	0.02 (0.03)	0 (0.02)	0.95 (0.86)	0.86 (0.71)
MATT	63	545	0.13	0.10	0.03 (0.04)	0.05 (0.08)	0 (0.01)	0.01 (0.03)	0.97 (0.95)	0.85 (0.73)
MANF	68	581	0.15	0.12	0.06 (0.05)	0.05 (0.06)	0 (0.02)	0.01 (0.02)	0.80 (0.83)	0.89 (0.82)

Note: rmse, μ, and ρ_0^2 are computed from differences between HFR and drifter radial velocities. For each value, the corresponding value evaluated without applying the measured antenna pattern is reported in parenthesis. rms of the velocities sensed by the drifters rms_d^R and time t_d spent by all the drifters within each radar coverage are reported as well.

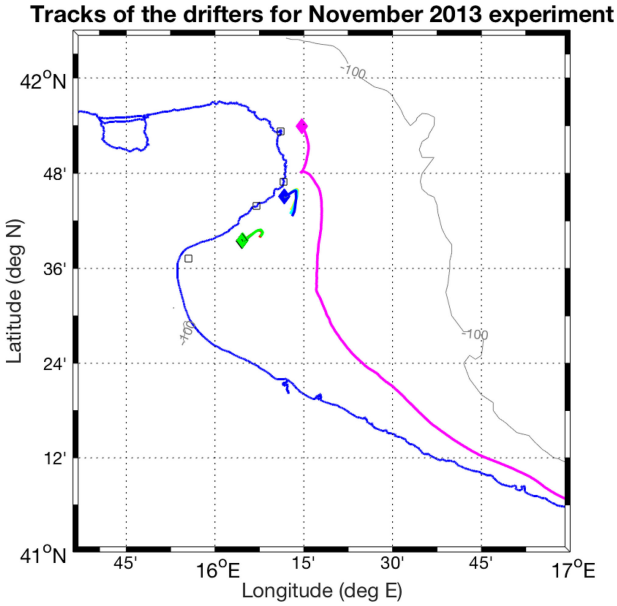

Fig. 9. Trajectories of the drifters launched during the November 2013 experiment. The two "short" tracks are drifter triplets. The diamond markers represent the release points.

the drifter residence times within the coverage. The drifters indeed stayed in the radar coverage for several days (up to 14 days) and t_d ranges between approximately 90 and 580 h (see Table III). Thus, the statistical significance of the comparison results is expected to be higher for the February data.

The comparison is performed considering velocities in the radial direction since radial velocities are directly measured by the HFRs. At this end, drifter velocities are projected on the radial direction, i.e., along the line of sight of each radar station. Radial velocities from HFRs (u_{HFR}^R) and from drifters (u_d^R) are compared at the same times and locations. Drifter data are resampled on the uniform radar time grid, and the radar velocity is estimated through bilinear interpolation of the radar velocities corresponding to the cells closest to each drifter position. The difference between the two estimated radial velocities is then calculated as $\Delta u^R = u_{\text{HFR}}^R - u_d^R$.

The statistics of the comparison are evaluated by averaging over all drifter positions at all times (the overbars stand for the average) in terms of bias $\mu = \overline{\Delta u^R}$, root-mean-square error $\text{rmse} = \sqrt{\overline{(\Delta u^R)^2}}$, and zero-lag correlation coefficients ρ_0^2 [75].

To test the effectiveness of antenna calibration, the same statistics have also been evaluated for HFR radial uncalibrated velocities, i.e., velocities measured without applying the measured antenna patterns. These quantities have been then compared to the calibrated ones, i.e., computed applying the measured antenna patterns in the bearing calculation process.

The rms of the radial velocities sensed by the drifters, evaluated as $\text{rms}_d^R = \sqrt{\overline{(u_d^R)^2}}$ (the overbar stands for the average), and the total times t_d spent by all the drifters within each radar site coverage have been computed as a term of reference to assess the statistical significance of the comparison experiments.

The comparison results are summarized in Table III for both experiments, where rmse, μ, and ρ_0^2 are computed for each radar station. For each value, the corresponding value evaluated without applying the measured antenna pattern is reported in parentheses.

For all sites and both experiments, the calibrated rmse lies in the range 0.03–0.08 m/s, well within what is considered acceptable in the literature [76].

The rmse values are significantly smaller than the rms value of the drifter velocities: for the November experiment, rmse values are $\approx 20\% - 40\%$ of the drifter rms, whereas for February, rmse values are $\approx 30\% - 50\%$ of the drifter rms.

Biases are 0 m/s for three out of four sites for the calibrated velocities, namely VIES, MATT, and MANF, for the November experiment, and two out of four sites, namely VIES and PUGN, for the February experiment. For both experiments, the nonzero biases are reasonably small (0.01 and 0.02 m/s) and much below the rmse.

A relevant question is which part of the discrepancy between drifters and HFR is due to the fact that the two platforms sample the natural variability of the flow in different ways. Ohlmann *et al.* [31] have estimated the variability at the scales of the HFR averages (i.e., at the grid size in space and at 1 h in time) by maintaining a coverage of $\approx$10 drifters within a fixed grid cell through repeated launches, and by averaging daily. The data set presented in this paper does not allow such a detailed estimation, but the analysis of the two November triplets can provide some useful information. Within each triplet, hourly averages of drifter relative distance, mean velocity, and std were evaluated. Drifters are found to maintain an average distance of $\approx$70–300 m within the two triplets during the measurement period, with an average std of 0.014 m/s. Since the distances between triplets cover scales smaller than the average radial

grid ($\approx$1.3 km^2), the std is likely to provide a lower bound for variability at the radar scale. It is interesting to notice that the std is of the same order that the bias (0.015 m/s) between the mean hourly velocity of the triplets and the HFR velocity within the same grid.

The zero-lag correlation coefficients show an excellent agreement in all sites between the velocities from radar and drifters. It can be noted that the correlation coefficients evaluated for the February experiment are generally lower than the ones for the November experiment (except that for MANF site). This might be only partially significant, given the small November data set. Nevertheless, a possible reason could be that during the November experiment, the synoptic currents were dominated by a large-scale pattern well resolved by the radar [see Fig. 2(a)], whereas in February, the synoptic circulation was more complex with several recirculations that might be only partially resolved by the radar grid [see Fig. 2(b)], making the differences with the drifters higher. It is interesting to notice that the November velocity pattern in Fig. 2(a) is consistent with the typical mean fall circulation (September 21 to December 21), dominated by a stable and extended WAC boundary current [38]. The mean winter circulation (December 21 to March 21) is still characterized by a prominent WAC, even though less extended and less stable than in the fall, whereas in spring (March 21 to June 21), the boundary current typically becomes weaker and the circulation is characterized by an enhanced spatial and temporal variability. The February synoptic currents in Fig. 2(b) are more similar to the typical spring conditions, suggesting a weakened WAC during the period of drifter release.

The evaluation of the effects of the antenna calibration confirms the expected improvement of the measuring reliability of the radar devices. All the statistics (rmse, μ, and ρ_0^2) improve in all cases, with the exception of rmse and ρ_0^2 for MANF in the November experiment, where a slight worsening has been recorded when applying the measured antenna pattern. Since the cross-loop pattern of the MANF antenna is the closest to the ideal shape [as shown in Fig. 4(b)], the differences between the calibrated and the uncalibrated measurements are expected to be reduced. In the February experiment, whose statistical significance is higher due to the longer time spent by the drifters in the radar coverage, the application of antenna pattern improves the accuracy of all the four radar stations.

In addition to these bulk quantities, also the regressions between drifter velocities and radar velocities with and without applying the measured antenna patterns have been computed at each site and for both experiments. Fig. 10 shows November results, whereas Fig. 11 shows the February results. Overall, the results confirm the good agreement between the surface currents measured by the HFR network and the ones measured by the surface drifters, and show the improvement related to the measured antenna pattern.

To evaluate the effectiveness of the applied QC, the comparison between drifter- and HFR-derived velocities has been performed also with the HFR data without QC. For this assessment only calibrated HFR velocities have been used.

Concerning the velocity threshold applied to radial data, it turned out that only 0.47% of the radial vectors (230 out of 48 498) were removed by the QC for the November experiment and none was removed (0 out of 79 178) by the QC for the February experiment. This is a consequence of the policy adopted by CNR-ISMAR of keeping conservative thresholds for velocity controls to remove only extreme outliers. The vectors removed by QC in the November experiment were not involved in the comparison with drifter velocities (because these vectors are lying in zones where the drifters did not pass). Thus, no difference in the comparison between the drifter data and the HFR data with and without velocity threshold QC has been recorded in the two experiments.

Drifters were also used to validate HFR total vectors, by comparing synthetic trajectories with observed drifter trajectories, to assess the reliability of HFR current fields for Lagrangian transport estimation. As previously done by Berta *et al.* [77], [78], the uncertainty on the transport estimate is quantified by the separation between drifters and synthetic trajectories. This quantity has to be considered together with the maximum uncertainty on particle position knowledge (represented by drifters absolute dispersion).

Synthetic trajectories were advected in the HFR field with a fourth-order Runge–Kutta scheme for 12 h (typical period for operational applications). All synthetic particles were reinitialized at the drifters location every 12 h. As depicted in Fig. 13, results show that, for both the experiments, the separation between observed and synthetic trajectories after 12-h ranges from 1 to 2 km, compared to about 8.5-km absolute dispersion. The uncertainty on HFR transport estimates is at least 75% lower than the absolute dispersion of drifters, implying good agreement between HFR total currents and observed drifters.

Again, the results of the November experiment are better than the ones of the February experiment, probably due to the presence of large scale patterns in the November synoptic currents, which are better resolved by the radars with respect to the small patterns present in the February synoptic field.

In practical terms, HFRs represent a strategic resource in many operational settings, such as maritime spatial planning, given that surface current measurements provide *a priori* knowledge on the coastal dynamics useful for sustainable integration of human activities in marine areas, for example, estimating larval transport to improve fisheries management in coastal environments.

IV. Correlation Between Surface and Water Column

ADCPs measure current speed and direction in the water column by transmitting high-frequency sound waves and determining the Doppler frequency shift of the return signal scattered from the water column [32]. Upward looking ADCPs typically provide velocities averaged within vertical cells of the order of meters, whose maximum range and resolution depend on the emitting frequency. The measurements taken in the near-surface volume are often discarded because they have the highest velocity SNR, due to the high surface echo intensity caused by turbulence and air bubbles.

As a consequence, given the high shear expected to occur in the surface layers [76], measurements from upward look-

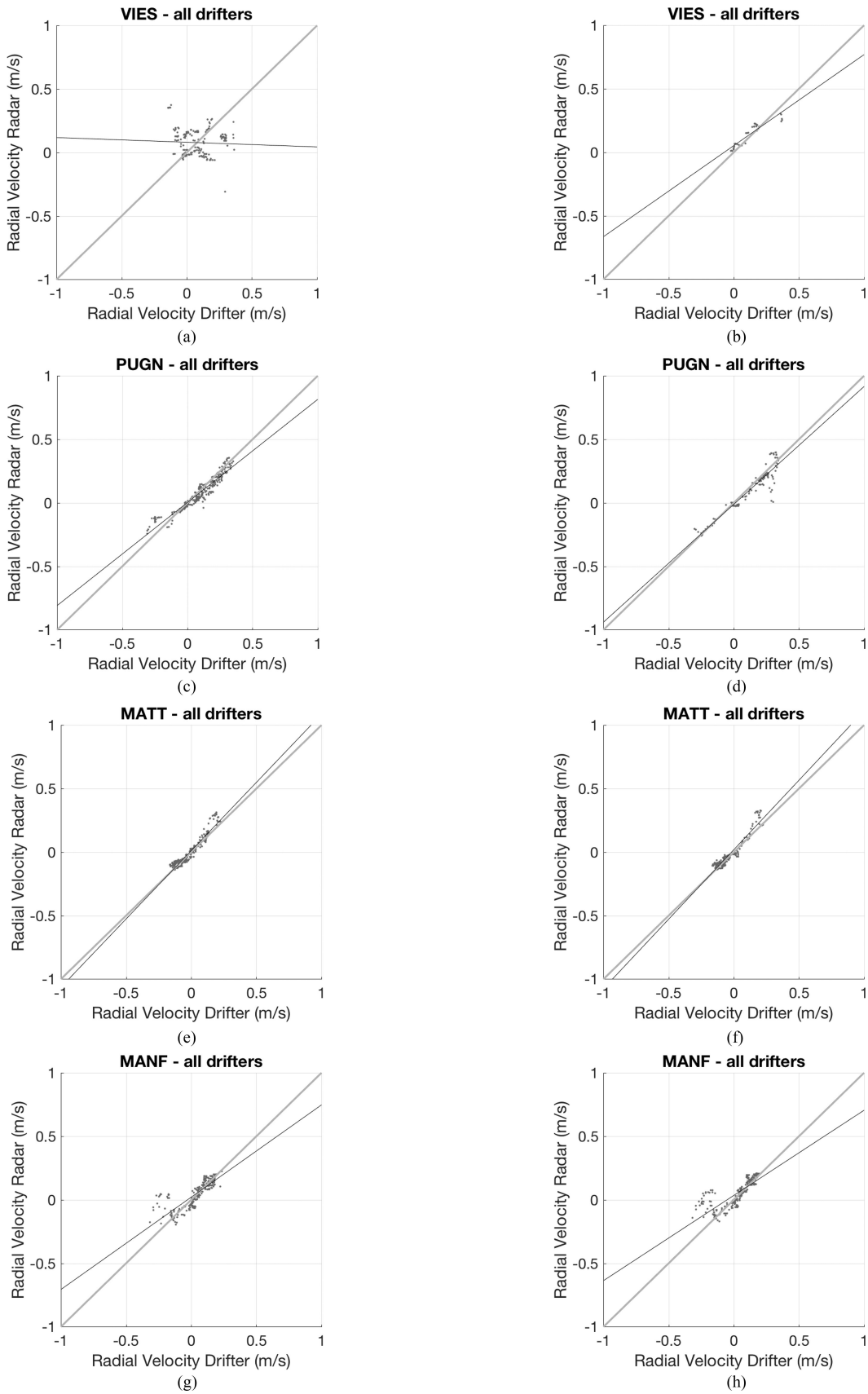

Fig. 10. Regressions between radar velocities sensed without (uncalibrated) and with (calibrated) applying the measured antenna patterns and drifter velocities at VIES, PUGN, MATT, and MANF site in the November 2013 experiment. (a) VIES uncalibrated. (b) VIES calibrated. (c) PUGN uncalibrated. (d) PUGN calibrated. (e) MATT uncalibrated. (f) MATT calibrated. (g) MANF uncalibrated. (h) MANF calibrated.

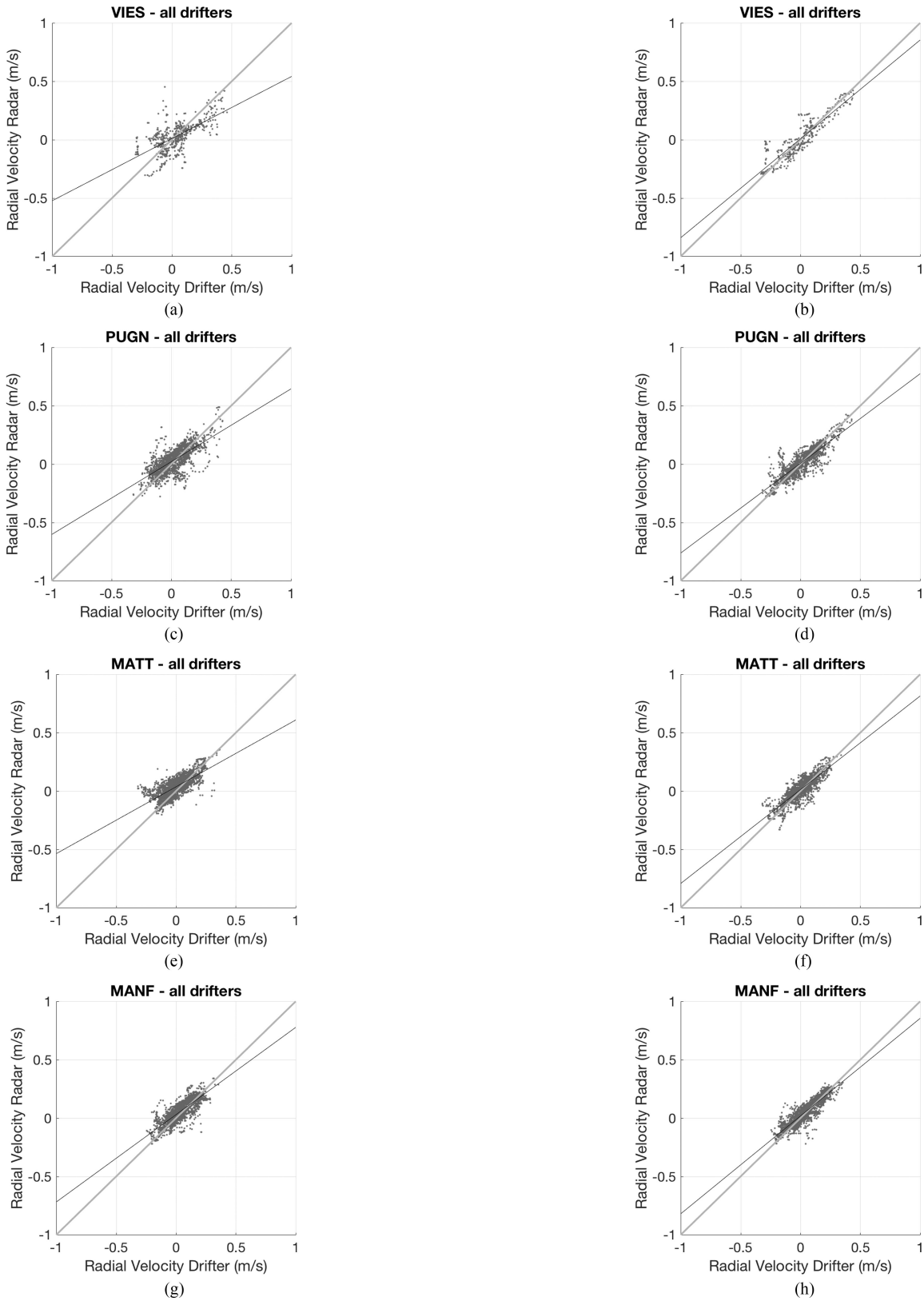

Fig. 11. Regressions between radar velocities sensed without (uncalibrated) and with (calibrated) applying the measured antenna patterns and drifter velocities at VIES, PUGN, MATT and MANF site in the February 2014 experiment. (a) VIES uncalibrated. (b) VIES calibrated. (c) PUGN uncalibrated. (d) PUGN calibrated. (e) MATT uncalibrated. (f) MATT calibrated. (g) MANF uncalibrated. (h) MANF calibrated.

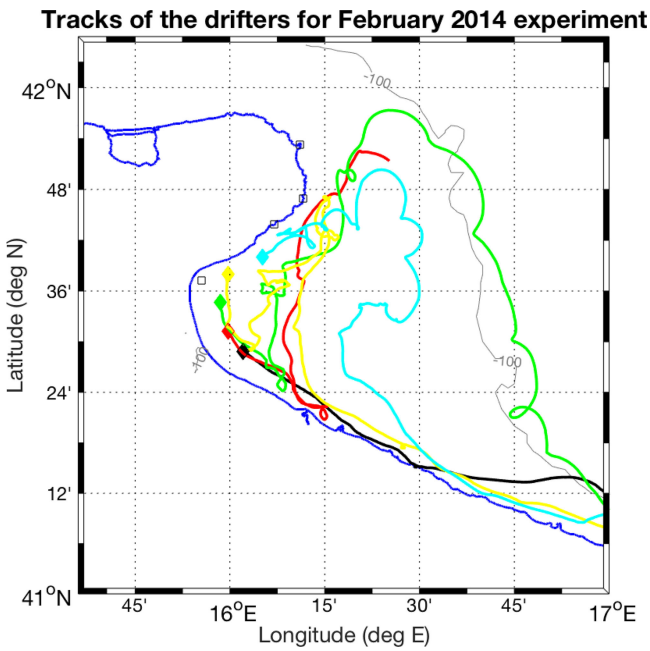

Fig. 12. Trajectories of the drifters launched during the February 2014 experiment. The diamond markers represent the release points.

TABLE IV
GEOGRAPHIC COORDINATES AND OPERATIONAL SETTINGS OF THE ADCP MOUNTED ON THE MEDA GARGANO

Position	41° 30.973' N - 16° 8.970' E
Operating frequency	750 kHz
Maximum range	40 m
Spatial resolution	0.8 m
Water velocity range	[-6 : 6] m/s
Water velocity resolution	0.001 m/s
Water velocity accuracy	0.005 m/s

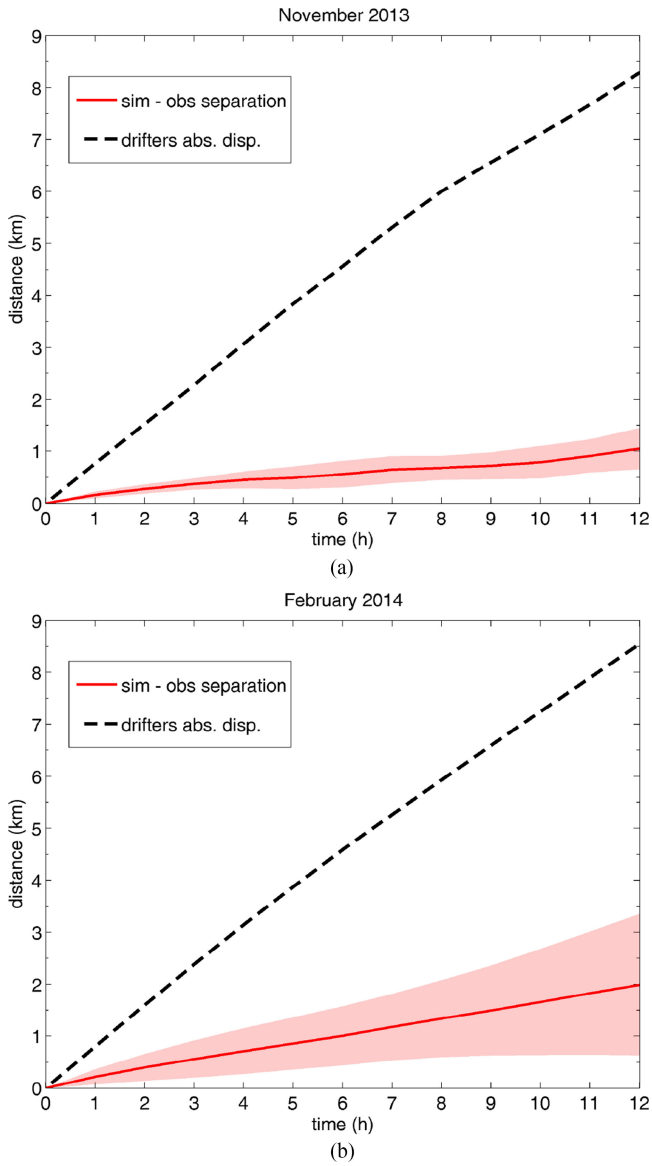

Fig. 13. Separation between observed (drifters) and simulated (HFR) trajectories for (a) November 2013 and (b) February 2014. The shade indicates std, while the black dashed line indicated drifters absolute dispersion.

ing ADCP are less compatible with HFR velocities than drifter measurements and not as suitable for validation. On the other hand, they provide very important additional information regarding the velocity profiles in the water column that complement the surface information from the HFR.

The ISMAR HFR network was deployed along the coast of Gargano Promontory with the aim of investigating dispersion and retention properties in the Gulf, with special interest for the advection of larvae of small pelagic fishes, such as sardines [34]. Since larvae of sardines move vertically in the upper 15–20 m of the water column, it is of great interest to complement the surface HFR velocities with ADCP information. In particular, it is important to verify whether the HFR information can be considered representative of the water column behavior. At this end, the comparison between HFR surface velocity and ADCP velocity in the Gulf was performed, concentrating on two periods during January and March 2015, when both measurements were available in the Gulf. The winter/spring season is especially interesting since it corresponds to the spawning season for sardines.

The ADCP was mounted on a seamark called Meda Gargano, installed within the coverage of the ISMAR HFR network (see Fig. 1), 12-mi offshore from the port of Manfredonia on a 17-m-deep seabed. Meda Gargano is an elastic seamark manufactured by Floatex, Provaglio d'Iseo, Italy, and its structure consists of a 25-m-long steel pole, 18 m of which is immersed and 7 m is above the sea surface. The pole is fixed to the seabed through a 30-t ballast. The seamark is operational since 2012 hosting scientific instrumentation, and the ADCP has been added in November 2014 to its payload.

The ADCP is a SonTek Argonaut-XR current profiler equipped with an upward looking three-beam transducer for measuring 3-D water velocity and it operates at a frequency of 750 kHz. Position coordinates and technical specifications are reported in Table IV. It measures zonal (u_{ADCP}) and meridional (v_{ADCP}) components of water velocity in three depth

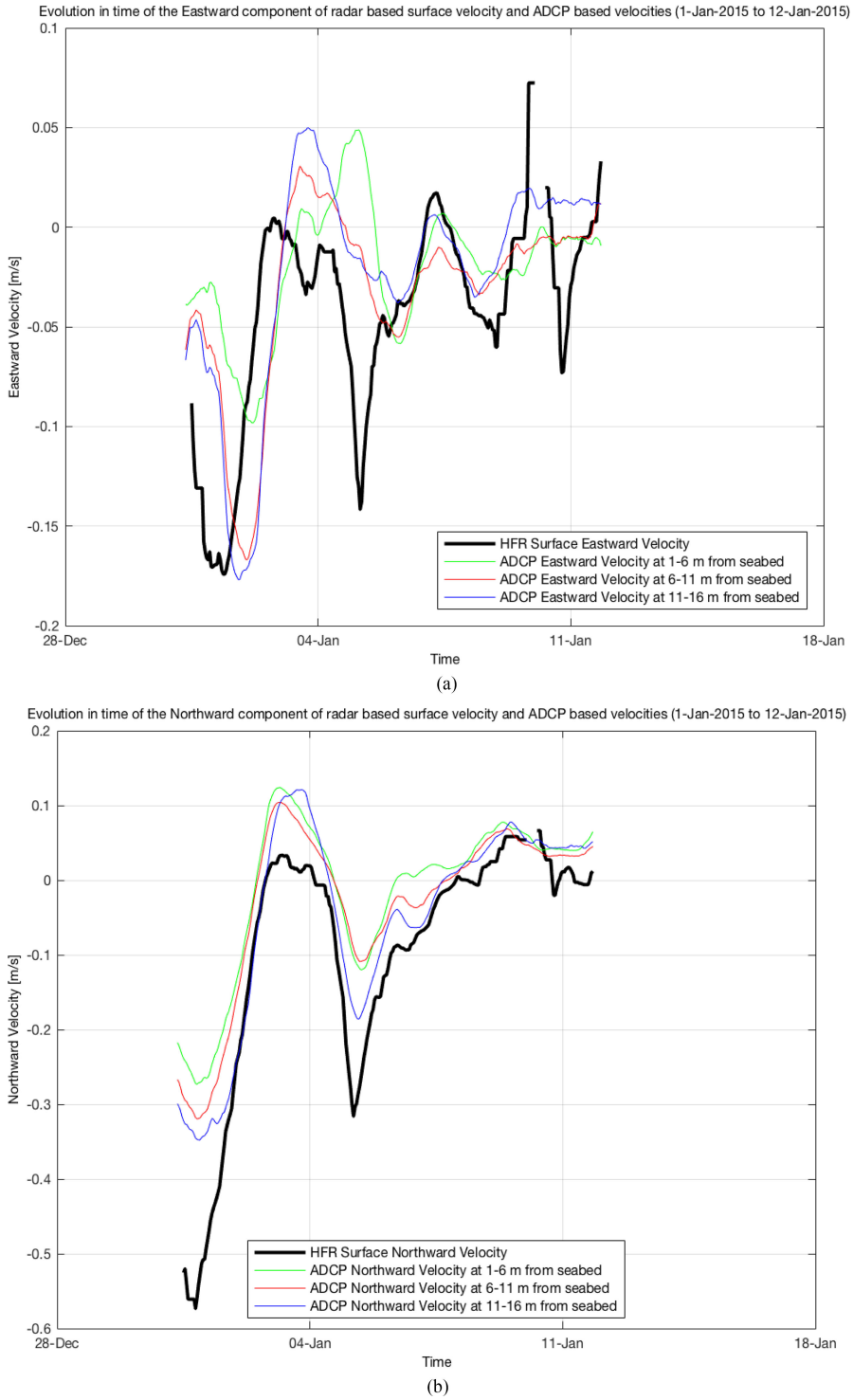

Fig. 14. Evolution in time of (a) u and (b) v components of current velocity as sensed by the HFR and by the ADCP in the three depth cells. The reference time period is January 1–12, 2015. The moving average function applied on HFR data is able to manage data gaps.

cells spanning 5 m of the water column each, with an accuracy of 0.005 m/s. Cell 1 covers the depth range 1–6 m from surface, cell 2 covers the depth range 6–11 m from surface, and cell 3 covers the depth range 11–16 m from surface. The first meter under the surface is not covered by any cell to avoid interferences caused by tides and waves. Water velocity measurements are sampled every 10 min in each cell. Each sample is quality controlled via a threshold on the signal strength level.

Two time series of the ADCP u_{ADCP} and v_{ADCP} velocity components were used for the comparison with the HFR velocities: the periods January 1–12, 2015 (10 368 ADCP

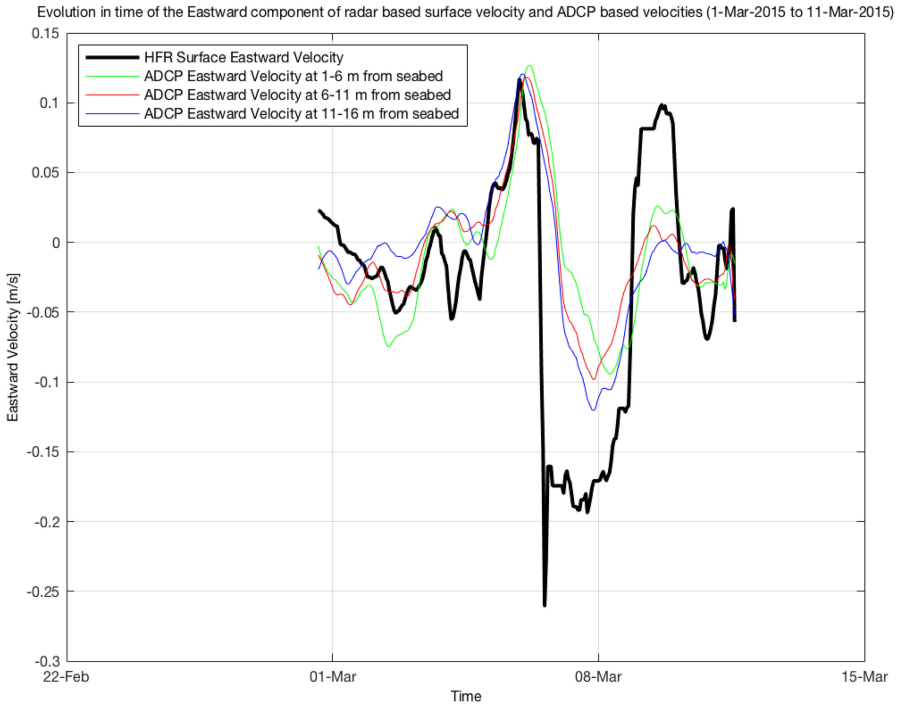

Fig. 15. Evolution in time of (a) u and (b) v components of current velocity as sensed by the HFR and by the ADCP in the three depth cells. The reference time period is March 1–11, 2015. The moving average function applied on HFR data is able to manage data gaps.

10-min measurements) and March 1–11, 2015 (9504 ADCP 10-min measurements).

The u_{HFR} and v_{HFR} components of the total velocities from HFRs and the u_{ADCP} and v_{ADCP} components of water velocities measured at each depth level from the ADCP are compared at the same time and locations. On the HFR side, velocity components in the grid cell where the seamark is located are extracted for comparison along the time series. The 10-min velocity components measured by the ADCP are averaged, separately for each depth cell, on the corresponding 1-h intervals

TABLE V
MAXIMUM CROSS CORRELATIONS $\rho^2_{u\_\mathrm{ADCP}}$ AND $\rho^2_{v\_\mathrm{ADCP}}$ AND CORRESPONDING TIME LAGS τ_{u_ADCP} AND τ_{v_ADCP} EVALUATED FOR THE u AND v COMPONENTS OF WATER VELOCITY MEASURED BY THE ADCP BETWEEN ADJACENT DEPTH LEVELS FROM SEA SURFACE FOR THE TWO PERIODS JANUARY 1–12, 2015 AND MARCH 1–11, 2015

Depth cell (m from surface)	$\rho^2_{u\_ADCP}$		$\rho^2_{v\_ADCP}$		τ_{u_ADCP} [hours]		τ_{v_ADCP} [hours]	
	Jan	Mar	Jan	Mar	Jan	Mar	Jan	Mar
Cell 1 ([1-6] m) vs Cell 2 ([6-11] m)	0.97	0.94	0.98	0.99	0	-1	0	1
Cell 2 ([6-11] m) vs Cell 3 ([11-16] m)	0.91	0.94	0.98	0.98	5	3	0	1

TABLE VI
RMS OF THE u AND v COMPONENTS OF WATER VELOCITY MEASURED BY HFR AND BY ADCP AT THE THREE DEPTH LEVELS FROM SEA SURFACE FOR THE TWO PERIODS 1–12 JANUARY 2015 AND 1–11 MARCH 2015

Depth cell (m from surface)	rms_u^{ADCP} [m/s]		rms_v^{ADCP} [m/s]		rms_u^{HFR} [m/s]		rms_v^{HFR} [m/s]	
	Jan	Mar	Jan	Mar	Jan	Mar	Jan	Mar
Cell 1 ([1-6] m)	0.074	0.067	0.158	0.157	0.0853	0.106	0.184	0.152
Cell 2 ([6-11] m)	0.068	0.063	0.128	0.147				
Cell 3 ([11-16] m)	0.053	0.072	0.118	0.134				

TABLE VII
MAXIMUM CROSS CORRELATIONS ρ^2_u AND ρ^2_v AND CORRESPONDING TIME LAGS τ_u AND τ_v EVALUATED BETWEEN HFR AND ADCP u AND v COMPONENT OF WATER VELOCITY AT THE SURFACE LEVEL (1–6 m FROM SURFACE) FOR THE TWO PERIODS 1–12 JANUARY 2015 AND 1–11 MARCH 2015

Depth cell (m from surface)	ρ^2_u		ρ^2_v		τ_u [hours]		τ_v [hours]	
	Jan	Mar	Jan	Mar	Jan	Mar	Jan	Mar
Cell 1 ([1-6] m)	0.83	0.76	0.95	0.95	-4	-10	0	1

to which HFR data are related. Before the comparative analysis, the two data series have been filtered with a 24-h moving average to filter out extremely high-frequency oscillations in the signals. The moving average function is able to manage data gaps [Not a Number (NaN)] to take into account the few and small gaps possibly present in the two data time series.

The time series of the ADCP u_{ADCP} and v_{ADCP} velocity components are shown in Figs. 14 and 15. Blue lines indicate cell 1, red lines cell 2, and green lines cell 3. In the same plots also time series of the HFR total velocity components u_{HFR} and v_{HFR} are shown (in black), corresponding to the grid cell where the seamark is located.

The time series have been statistically analyzed and the results are summarized in Tables V–VII.

Concerning the structure of the water column velocity profiles as depicted by ADCP measurements, visual inspection of Figs. 14 and 15 suggests an overall consistency of the velocities in the three cells, indicating homogeneous conditions as it can be expected in the winter/early spring season.

This qualitative assessment is confirmed by the computation of the maximum cross correlations ($\rho^2_{u\_\mathrm{ADCP}}$ and $\rho^2_{v\_\mathrm{ADCP}}$) and time lags (τ_{u_ADCP} and τ_{v_ADCP}) [79] between adjacent depth cells shown in Table V for the two periods. The ρ^2 values are high, ranging between 0.99 and 0.91, with time lags of 1–5 h. The worse result is obtained for the u correlation between cells 2 and 3 in January ($\rho^2_{u\_\mathrm{ADCP}} = 0.91$, $\tau_{u_\mathrm{ADCP}} = 5$h), and it is likely related to an episode around January 5 [see Fig. 14(a)], when cell 3 (green line) shows a peak that is not present in the other cells. In fact the signal strength level was very low in cell 1 on January 5. It has to be noted that the applied correlation function is able to manage NaNs, to take into account possible data gaps.

Regarding the energetics of the flow, the rms of the ADCP-based velocity components have been evaluated as $\mathrm{rms}_u^{\mathrm{ADCP}} = \sqrt{\overline{(u_{\mathrm{ADCP}})^2}}$ and $\mathrm{rms}_v^{\mathrm{ADCP}} = \sqrt{\overline{(v_{\mathrm{ADCP}})^2}}$ (the overbar stands for the average), and are shown in Table VI for the three cells and the two periods. The rms decreases from the top to the bottom cells in all cases, except for u_{ADCP} in March, when the bottom cell is the most energetic one in the water column. It is also noticeable that the zonal velocities are less energetic than the meridional ones (of more than 50%).

When comparing the water column velocities with the surface velocities from the HFR, it comes out that rms velocities from HFRs ($\mathrm{rms}_u^{\mathrm{HFR}} = \sqrt{\overline{(u_{\mathrm{HFR}})^2}}$ and $\mathrm{rms}_v^{\mathrm{HFR}} = \sqrt{\overline{(v_{\mathrm{HFR}})^2}}$) are higher than ADCP's in most cases (see Table VI), as it can be expected given that the surface layer is in direct contact with atmospheric forcing. In particular, the HFR rms exceeds the ones in cell 1 by $\approx 36\% - 13\%$, except for the case of v during March, when HFR is slightly lower (of approximately 3%).

TABLE VIII
MAXIMUM CROSS CORRELATIONS ρ_u^2 AND ρ_v^2 AND CORRESPONDING TIME LAGS τ_u AND τ_v EVALUATED BETWEEN HFR WITH AND WITHOUT GDOP THRESHOLD QC AND ADCP u AND v COMPONENT OF WATER VELOCITY AT THE SURFACE LEVEL (1–6 m FROM SURFACE) FOR THE TWO PERIODS 1–12 JANUARY 2015 AND 1–11 MARCH 2015

Depth cell (m from surface)	ρ_u^2		ρ_v^2		τ_u [hours]		τ_v [hours]	
	Jan	Mar	Jan	Mar	Jan	Mar	Jan	Mar
GDOP QC	0.83	0.76	0.95	0.95	-4	-10	0	1
No GDOP QC	0.57	0.39	0.78	0.93	8	15	11	1

The maximum cross correlations (ρ_u^2 and ρ_v^2) and time lags (τ_u and τ_v) between HFR and ADCP cell 1 velocities are shown in Table VII. The values for the meridional component are very good ($\rho_v^2 = 0.95$, $\tau_v = 0$–1 h), as it is also evident from the time series in Figs. 14(b) and 15(b). For the less energetic zonal component, the correlation is still good but lower ($\rho_u^2 = 0.83-0.76$, $\tau_u = -4$–10 h).

The meridional component of the flow v is likely to be directly influenced by the WAC especially in fall and winter [38], despite the fact that the ADCP is located quite internally in the Gulf. As a consequence, v is expected to be more energetic than the zonal component u and influenced by large-scale WAC dynamics. Zonal fluctuations, on the other hand, are more likely to be related to more local phenomena, such as local winds, river inflows, and nonlinear recirculating cells. Local phenomena might be less correlated in the vertical, explaining the differences between surface and water column velocities. As an example, the two main southward episodes around January 5 (see Fig. 14) and around March 6 (see Fig. 15) occur during events of northerly winds, as evaluated by the COSMO-7 wind model reanalysis. These data, not shown in this paper, are gridded data with 6.6-km resolution and have a 1-h temporal resolution. For each hour of the two experiments, they have been averaged on the HFR coverage and compared with the ADCP and HFR measurements. During the mentioned wind events, that are expected to reinforce the WAC and its penetration in the Gulf [39], the currents show a good vertical correlation in the meridional component. The January 5 episode, though, also shows a zonal anticorrelation between the HFR and cell 3 velocities, that is not easily explainable. The dynamics in the Gulf is indeed quite complex and its description and understanding is outside the scope of this paper.

In summary, the results show that, at least in the considered period, the more energetic meridional component is very well correlated from the surface to the bottom of the water column, with decreasing velocities toward the bottom. The zonal component is also characterized by good correlation values, but there are a few episodes when the interior velocities, especially closer to the bottom, behave differently from the surface ones. These results are expected to play an important role for biological applications since they suggest that surface circulation and larvae transport results from HFR can be significant also for transport in the water column during winter, for instance, considering a velocity attenuation coefficient with depth [34]. These aspects will need further testing with additional data, but they set the way toward interesting developments.

To evaluate the performances of the applied QC, the comparison between ADCP and HFR derived velocities has been performed also with HFR data without QC.

The velocity threshold applied to total data does not affect any of the vectors located in the ADCP grid cell, thus no difference in the comparison between ADCP data and HFR data with and without velocity threshold QC has been recorded in the two experiments. As mentioned in Section III, this is a consequence of the conservative threshold policy of CNR-ISMAR for QC.

On the other hand, the GDOP threshold QC removed 16.54% (42 out of 254) of the total vectors used for comparison with ADCP in the January experiment and 7.02% (16 out of 228) of the total vectors used in the March experiment. Based on this fact, the comparison between ADCP velocities and HFR velocities without GDOP threshold QC has been performed and it proved that the QC improves the quality of the HFR data since the comparison using data not quality controlled gives worse results with respect to the ones obtained with quality controlled data, as shown in Table VIII.

V. SUMMARY AND CONCLUSION

The ISMAR HFR network for the measurement of the velocity of surface currents in coastal seas has been operational on the coasts of the Southern Adriatic Sea in 2013–2015. The network has covered an area of approximately 1700 skm^2 in the Gulf of Manfredonia, providing high-level performances in terms of temporal and spatial coverage, optimal geometrical configuration (necessary for radial combination into total vectors), SNR, and NF. The measurement and data production pipelines operated under QA/QC procedures.

The network provided hourly surface velocity fields, both radial velocities and total velocities, in real-time mode and data were produced in interoperable formats, according to the standards of OGC for the access and delivery of geospatial data, adherent to the US ROWG recommendations and compliant to the CF Metadata Conventions CF-1.6 and the INSPIRE directive.

Data were distributed via a THREDDS catalog supporting OGC compliant distributions and protocols for data visualization, metadata interrogation, and data download. The access to data is free and it is licensed under a Creative Commons Attribution 4.0 International License.

The surface current velocities sensed by the ISMAR HFR network have been compared with velocities measured by drifters deployed within the radar coverage. The comparison results

show the rms of velocity differences (0.03–0.08 m/s) corresponding to ≈20%–50% of the drifter rms, lying on the low end of the range considered acceptable in literature given the expected variability at the HFR subgrid scale. Biases are low (0–0.02 m/s) while high correlation (0.85–0.97) between HFR and drifter based velocities was found. Results show the expected improvements due to antenna calibration.

The drifters deployed in triplets have been used to provide a lower bound for the variability at radar scale since the distances between the drifters in the triplets covered scales smaller than the radial grid size.

Drifter velocities were also used to validate HFR total vectors, by comparing synthetic trajectories, evaluated from HFR velocity fields, with observed drifter trajectories, to assess the reliability of HFR current fields for Lagrangian transport estimation. The uncertainty on the transport estimate is quantified by the separation between drifters and synthetic trajectories. Results show that, for both the experiments, the separation between observed and synthetic trajectories after 12 h ranges from 1 to 2 km, compared to about 8.5-km absolute dispersion. The uncertainty on HFR transport estimates is at least 75% lower than the absolute dispersion of drifters, implying good agreement between HFR total currents and observed drifters.

Surface velocity from HFR is also compared with water column velocity profiles from an upward looking ADCP operating in the Gulf at 17-m depth during two periods in January and March. Results show that the water column is well correlated with the surface, especially in the meridional component, that represents the most energetic and prevalent part of the flow (correlation of 0.95). The overall correlation values are also good for the zonal component (0.83–0.75), but there are episodes when surface and bottom flows are decorrelated.

The comparison between ADCP and HFR derived velocities has been performed using both HFR data with and without QC, to evaluate the performances of the applied QC procedures. This analysis proved that the QC improves the quality of the HFR data since the comparison using quality controlled HFR data gives better results with respect to the ones obtained with data not quality controlled.

The data produced by the ISMAR HFR network are presently used in a number of applications, ranging from fishery to coastal management. For all these applications, validation and data QC are of course essential, but also the comparison with water column data is relevant to understand whether or not the HFR velocities can be considered representative also of the subsurface flow. The present results indicate that this is the case for winter/spring conditions, which are relevant for fishery applications to sardine larvae dispersion since the season corresponds to sardine spawning time. It should be noted that the situation is expected to be different in the presence of significant stratification, for instance for different seasons or in the presence of strong river outflows.

Recently, significant efforts have been devoted in Europe toward the homogenization of various research-driven HFR networks present in different European countries, to establish a unified European coastal radar network. The ISMAR network is part of the RITMARE Italian coastal radar network and CNR-ISMAR represents the Italian partners as a member of the EuroGOOS HFR Task Team, responsible to set the foundation of the unified European network.

Within these frameworks, the Gulf of Manfredonia network has been instrumental to set up of a core of QC practices and interoperable data and metadata formats that have been subsequently used within the Italian RITMARE network and that are presently discussed and refined at the European level through the projects Jerico-NEXT and INCREASE.

ACKNOWLEDGMENT

The authors would like to thank the RITMARE, Co.Co.Net, SSD Pesca, and Jerico-NEXT projects, the Institute of Atmospheric Sciences and Climate of the National Research Council of Italy (CNR-ISAC), the University of Naples "Parthenope," CoNiSMa, and the Physical and Chemical Oceanography Group of the Department of Marine Sciences at the University of the Aegean, Mytilini, Greece, for the support to the research.

REFERENCES

[1] J. Harlan *et al.*, "The integrated ocean observing system high-frequency radar network: Status and local, regional, and national applications," *Mar. Technol. Soc. J.*, vol. 44, no. 6, pp. 122–132, 2010.

[2] D. D. Crombie, "Doppler spectrum of sea echo at 13.56 Mc./s.," *Nature*, vol. 175, pp. 681–682, 1955.

[3] D. E. Barrick, M. Evans, and B. Weber, "Ocean surface currents mapped by radar," *Science*, vol. 198, no. 4313, pp. 138–144, 1977.

[4] D. E. Barrick, "Extraction of wave parameters from measured HF radar sea-echo Doppler spectra," *Radio Sci.*, vol. 12, no. 3, pp. 415–424, 1977.

[5] D. Barrick and B. Lipa, "Comparison of direction-finding and beamforming in HF radar ocean surface current mapping," *Proc. Codar Ocean Sensors*, Los Altos, CA, USA, 1996, vol. 1.

[6] C. C. Teague, J. F. Vesecky, and D. M. Fernandez, "HF radar instruments, past to present," *Oceanography*, vol. 10, pp. 40–44, 1997.

[7] J. D. Paduan and L. Washburn, "High-Frequency radar observations of ocean surface currents," *Annu. Rev. Mar. Sci.*, vol. 5, pp. 115–136, 2013.

[8] R. H. Stewart and J. W. Joy, "HF radio measurements of surface currents," in *Deep Sea Research and Oceanographic Abstracts*, vol. 21, no. 12. New York, NY, USA: Elsevier, 1974, pp. 1039–1049.

[9] R. Chapman *et al.*, "On the accuracy of HF radar surface current measurements: Intercomparisons with ship-based sensors," *J. Geophys. Res., Oceans*, vol. 102, no. C8, pp. 18737–18748, 1997.

[10] D. Barrick, "Geometrical dilution of statistical accuracy (GDOSA) in multi-static HF radar networks, codar ocean sensors," Mountain View, CA, USA, 2002. [Online]. Available: http://www.codaros.com/Manuals/SeaSonde/Docs/Informative/GDOSA_Definition.pdf

[11] K.-W. Gurgel, Y. Barbin, and T. Schlick, "Radio frequency interference suppression techniques in FMCW modulated HF radars," in *Proc. OCEANS Europe*, Aberdeen, U.K., 2007, pp. 1–4.

[12] J. T. Kohut and S. M. Glenn, "Improving HF radar surface current measurements with measured antenna beam patterns," *J. Atmos. Ocean. Technol.*, vol. 20, no. 9, pp. 1303–1316, 2003.

[13] K. Laws, J. D. Paduan, and J. Vesecky, "Estimation and assessment of errors related to antenna pattern distortion in CODAR SeaSonde high-frequency radar ocean current measurements," *J. Atmos. Ocean. Technol.*, vol. 27, no. 6, pp. 1029–1043, 2010.

[14] M. Yaremchuk and A. Sentchev, "Mapping radar-derived sea surface currents with a variational method," *Continental Shelf Res.*, vol. 29, no. 14, pp. 1711–1722, 2009.

[15] D. M. Kaplan and F. Lekien, "Spatial interpolation and filtering of surface current data based on open-boundary modal analysis," *J. Geophys. Res., Oceans*, vol. 112, no. C12, pp. 1–20, 2007.

[16] B. Lipphardt, A. Kirwan, C. Grosch, J. Lewis, and J. Paduan, "Blending HF radar and model velocities in Monterey Bay through normal mode analysis," *J. Geophys. Res., Oceans*, vol. 105, no. C2, pp. 3425–3450, 2000.

[17] D. Barrick, V. Fernandez, M. I. Ferrer, C. Whelan, and Ø. Breivik, "A short-term predictive system for surface currents from a rapidly deployed coastal HF radar network," *Ocean Dyn.*, vol. 62, no. 5, pp. 725–740, 2012.

[18] J. O'Donnell *et al.*, "Integration of coastal ocean dynamics application Radar (CODAR) and short-term predictive system (STPS): Surface current estimates into the search and rescue optimal planning system (SAROPS)," Def. Tech. Inf. Center, Fort Belvoir, VA, USA, Tech. Rep. ADA444766, 2005, DTIC Document.

[19] E. Fredj, H. Roarty, J. Kohut, M. Smith, and S. Glenn, "Gap filling of the coastal ocean surface currents from HFR data: Application to the Mid-Atlantic Bight HFR Network," *J. Atmos. Ocean. Technol.*, vol. 33, no. 6, pp. 1097–1111, 2016. [Online]. Available: http://dx.doi.org/10.1175/JTECH-D-15-0056.1

[20] S. Y. Kim, E. Terrill, and B. Cornuelle, "Objectively mapping HF radar-derived surface current data using measured and idealized data covariance matrices," *J. Geophys. Res., Oceans*, vol. 112, no. C6, pp. 1–16, 2007.

[21] D. F. Carlson, P. A. Muscarella, H. Gildor, B. L. Lipphardt, and E. Fredj, "How useful are progressive vector diagrams for studying coastal ocean transport?" *Limnology Oceanogr., Methods*, vol. 8, no. 3, pp. 98–106, 2010.

[22] B. Zelenke *et al.*, "Evaluating connectivity between marine protected areas using CODAR high-frequency radar," in *Proc. OCEANS*, Biloxi, MS, USA, 2009, pp. 1–10.

[23] Ø. Breivik, A. A. Allen, C. Maisondieu, and M. Olagnon, "Advances in search and rescue at sea," *Ocean Dyn.*, vol. 63, no. 1, pp. 83–88, 2013.

[24] E. Fredj, D. F. Carlson, Y. Amitai, A. Gozolchiani, and H. Gildor, "The particle tracking and analysis toolbox (patato) for MATLAB," *Limnology Oceanogr., Methods*, vol. 14, no. 9, pp. 586–599, 2016. [Online]. Available: http://dx.doi.org/10.1002/lom3.10114

[25] M. Berta *et al.*, "Estimating Lagrangian transport blending drifters with HF radar data and models: Results from the TOSCA experiment in the Ligurian current (North Western Mediterranean Sea)," *Prog. Oceanogr.*, vol. 128, pp. 15–29, 2014. [Online]. Available: http://www.sciencedirect.com/science/article/pii/S007966111400127X

[26] J. Marmain, A. Molcard, P. Forget, A. Barth, and Y. Ourmières, "Assimilation of HF radar surface currents to optimize forcing in the northwestern Mediterranean Sea," *Nonlinear Processes Geophys.*, vol. 21, no. 3, pp. 659–675, 2014. [Online]. Available: http://www.nonlin-processes-geophys.net/21/659/2014/

[27] I. Shulman and J. D. Paduan, "Assimilation of HF radar-derived radials and total currents in the Monterey Bay area," *Deep Sea Res., II, Topical Stud. Oceanogr.*, vol. 56, no. 3, pp. 149–160, 2009.

[28] M. Berta *et al.*, "Improved surface velocity and trajectory estimates in the Gulf of Mexico from blended satellite altimetry and drifter data," *J. Atmos. Ocean. Technol.*, vol. 32, no. 10, pp. 1880–1901, 2015.

[29] A. Molcard *et al.*, "Comparison between VHF radar observations and data from drifter clusters in the Gulf of La Spezia (Mediterranean Sea)," *J. Mar. Syst.*, vol. 78, pp. S79–S89, 2009.

[30] R. E. Davis, "Drifter observations of coastal surface currents during CODE: The statistical and dynamical views," *J. Geophys. Res., Oceans*, vol. 90, no. C3, pp. 4756–4772, 1985.

[31] C. Ohlmann, P. White, L. Washburn, B. Emery, E. Terrill, and M. Otero, "Interpretation of coastal HF radar-derived surface currents with high-resolution drifter data," *J. Atmos. Ocean. Technol.*, vol. 24, no. 4, pp. 666–680, 2007.

[32] R. E. Thomson and W. J. Emery, *Data Analysis Methods in Physical Oceanography*. Oxford, U.K.: Newnes, 2014.

[33] Y. Liu, R. H. Weisberg, and L. K. Shay, "Current patterns on the West Florida shelf from joint self-organizing map analyses of HF radar and ADCP data," *J. Atmos. Ocean. Technol.*, vol. 24, no. 4, pp. 702–712, 2007.

[34] R. Sciascia *et al.*, "Linking sardine recruitment in coastal areas to ocean currents using surface drifters and HF radar. A case study in the Gulf of Manfredonia, Adriatic Sea," *Prog. Oceanogr.*, to be published, 2017.

[35] L. Corgnati *et al.*, "The ISMAR high frequency coastal radar network: Monitoring surface currents for management of marine resources," in *Proc. OCEANS 2015*, Genoa, Italy, 2015, pp. 1–8.

[36] P.-M. Poulain, "Adriatic sea surface circulation as derived from drifter data between 1990 and 1999," *J. Mar. Syst.*, vol. 29, no. 1, pp. 3–32, 2001.

[37] P. Falco, A. Griffa, P.-M. Poulain, and E. Zambianchi, "Transport properties in the Adriatic Sea as deduced from drifter data," *J. Phys. Oceanogr.*, vol. 30, no. 8, pp. 2055–2071, 2000.

[38] M. Veneziani, A. Griffa, and P.-M. Poulain, "Historical drifter data and statistical prediction of particle motion: A case study in the Central Adriatic Sea," *J. Atmos. Ocean. Technol.*, vol. 24, no. 2, pp. 235–254, 2007.

[39] M. G. Magaldi, T. M. Özgökmen, A. Griffa, and M. Rixen, "On the response of a turbulent coastal buoyant current to wind events: The case of the Western Adriatic Current," *Ocean Dyn.*, vol. 60, no. 1, pp. 93–122, 2010.

[40] D. F. Carlson *et al.*, "Observed and modeled surface Lagrangian transport between coastal regions in the Adriatic Sea with implications for marine protected areas," *Continental Shelf Res.*, vol. 118, pp. 23–48, 2016.

[41] A. Specchiulli *et al.*, "The role of forcing agents on biogeochemical variability along the southwestern Adriatic coast: The Gulf of Manfredonia case study," *Estuarine, Coastal Shelf Sci.*, vol. 183, pp. 136–149, 2016.

[42] L. Corgnat *et al.*, "The RITMARE Italian coastal radar network: Operational system and data interoperability framework," in *Proc. 7th EuroGOOS Conf.*, Lisbon, Portugal, 2016, pp. 1–7.

[43] A. Rubio *et al.*, "HF radar activity in European coastal seas: Next steps towards a Pan-European HF radar network," *Frontiers Mar. Sci.*, vol. 4, pp. 1–8, 2017.

[44] D. M. Fernandez and J. D. Paduan, "Simultaneous CODAR and OSCR measurements of ocean surface currents in Monterey Bay," in *Proc. Int. Geosci. Remote Sens. Symp.*, Lincoln, NE, USA, 1996, vol. 3, pp. 1749–1752.

[45] R. O. Schmidt, "Multiple emitter location and signal parameter estimation," *IEEE Trans. Antennas Propag.*, vol. 34, no. 3, pp. 276–280, Mar. 1986.

[46] B. Lipa, B. Nyden, D. S. Ullman, and E. Terrill, "SeaSonde radial velocities: Derivation and internal consistency," *IEEE J. Ocean. Eng.*, vol. 31, no. 4, pp. 850–861, Oct. 2006.

[47] Y. Abramovich, B. Johnson, and X. Mestre, "DOA estimation in the small-sample threshold region," in *Classical and Modern DOA Estimation*. Amsterdam, The Netherlands: Elsevier, 2009, ch. 7, pp. 219–287.

[48] E. Terrill *et al.*, "Data management and real-time distribution in the HF-radar national network," in *Proc. OCEANS*, Boston, MA, USA, 2006, pp. 1–6.

[49] R. Pawlowicz, "M_map: A mapping package for MATLAB," Dept. Earth Ocean Atmos. Sci., Univ. Brit. Columbia, Vancouver, BC, Canada, 2000, [Online]. Available: http://www.eos.ubc.ca/rich/map.html

[50] B. Lipa and D. Barrick, "Least-squares methods for the extraction of surface currents from CODAR crossed-loop data: Application at ARSLOE," *IEEE J. Ocean. Eng.*, vol. 8, no. 4, pp. 226–253, Oct. 1983.

[51] K.-W. Gurgel, "Shipborne measurement of surface current fields by HF radar," in *Proc. OCEANS'94, Oceans Eng. Today's Technol. Tomorrow's Preservation*, Brest, France, 1994, vol. 3, pp. III/23–III/27.

[52] H. C. Graber, B. K. Haus, R. D. Chapman, and L. K. Shay, "HF radar comparisons with moored estimates of current speed and direction: Expected differences and implications," *J. Geophys. Res., Oceans*, vol. 102, no. C8, pp. 18749–18766, 1997.

[53] M. Botts, G. Percivall, C. Reed, and J. Davidson, "OGC sensor web enablement: Overview and high level architecture," in *GeoSensor Networks*. New York, NY, USA: Springer, 2008, pp. 175–190.

[54] J. Gregory, "The CF metadata standard," *CLIVAR Exchanges*, vol. 8, no. 4, pp. 1–5, 2003.

[55] G. Bartha and S. Kocsis, "Standardization of geographic data: The European inspire directive," *Eur. J. Geography*, vol. 2, no. 2, pp. 79–89, 2011.

[56] H. Roarty, M. Smith, J. Kerfoot, J. Kohut, and S. Glenn, "Automated quality control of high frequency radar data," in *Proc. Oceans*, Hampton Roads, VA, USA, 2012, pp. 1–7.

[57] O. Bukhres, Z. B. Miled, E. Lynch, L. Olsen, and Z. Tari, "Effective standards for metadata in the GCMD data access system," in *Proc. Int. Symp. Distrib. Objects Appl.*, Antwerp, Belgium, 2000, pp. 155–161.

[58] P. Diviacco, A. Leadbetter, and H. Glaves, *Oceanographic and Marine Cross-Domain Data Management for Sustainable Development*. Hershey, PA, USA: IGI Global, 2016.

[59] P. Cornillon, J. Caron, T. Burk, and D. Holloway, "Data access interoperability within IOOS," in *Proc. OCEANS MTS/IEEE*, Washington, DC, USA, 2005, pp. 1790–1792.

[60] P.-M. Poulain, "Drifter observations of surface circulation in the Adriatic Sea between December 1994 and March 1996," *J. Mar. Syst.*, vol. 20, no. 1, pp. 231–253, 1999.

[61] P.-M. Poulain, L. Ursella, and F. Brunetti, "Direct measurements of water-following characteristics of CODE surface drifters," in *Proc. LAPCOD Meeting*, Key Largo, FL, USA, 2002, pp. 1–13.

[62] J. D. Paduan and L. K. Rosenfeld, "Remotely sensed surface currents in Monterey Bay from shore-based HF radar (coastal ocean dynamics application radar)," *J. Geophys. Res., Oceans*, vol. 101, no. C9, pp. 20669–20686, 1996.

[63] L. K. Shay, T. N. Lee, E. J. Williams, H. C. Graber, and C. G. Rooth, "Effects of low-frequency current variability on near-inertial submesoscale vortices," *J. Geophys. Res., Oceans*, vol. 103, no. C9, pp. 18691–18714, 1998.
[64] L. K. Shay, S. J. Lentz, H. C. Graber, and B. K. Haus, "Current structure variations detected by high-frequency radar and vector-measuring current meters," *J. Atmos. Ocean. Technol.*, vol. 15, no. 1, pp. 237–256, 1998.
[65] H.-H. Essen, K.-W. Gurgel, and T. Schlick, "On the accuracy of current measurements by means of HF radar," *IEEE J. Ocean. Eng.*, vol. 25, no. 4, pp. 472–480, Oct. 2000.
[66] L. K. Shay, T. M. Cook, Z. R. Hallock, B. K. Haus, H. C. Graber, and J. Martinez, "The strength of the M_2 tide at the Chesapeake Bay mouth," *J. Phys. Oceanogr.*, vol. 31, no. 2, pp. 427–449, 2001.
[67] B. M. Emery, L. Washburn, and J. A. Harlan, "Evaluating radial current measurements from CODAR high-frequency radars with moored current meters*," *J. Atmos. Ocean. Technol.*, vol. 21, no. 8, pp. 1259–1271, 2004.
[68] D. M. Kaplan, J. Largier, and L. W. Botsford, "HF radar observations of surface circulation off Bodega Bay (Northern California, USA)," *J. Geophys. Res., Oceans*, vol. 110, no. C10, pp. 1–25, 2005.
[69] J. D. Paduan, K. C. Kim, M. S. Cook, and F. P. Chavez, "Calibration and validation of direction-finding high-frequency radar ocean surface current observations," *IEEE J. Ocean. Eng.*, vol. 31, no. 4, pp. 862–875, Oct. 2006.
[70] I. I. Rypina, A. R. Kirincich, R. Limeburner, and I. A. Udovydchenkov, "Eulerian and Lagrangian correspondence of high-frequency radar and surface drifter data: Effects of radar resolution and flow components," *J. Atmos. Ocean. Technol.*, vol. 31, no. 4, pp. 945–966, 2014.
[71] P. Poulain *et al.*, "Mediterranean surface drifter database: 2 June 1986 to 11 November 1999," *Rel*, vol. 75, p. 2004, 2004.
[72] R. Gerin and A. Bussani, "Nuova procedura di editing automatico dei dati drifter impiegata su oceano per MyOcean e prodotti web in near-real time e delay mode," in *Proc. REL. OGS*, vol. 55, 2011, pp. 1–13.
[73] D. V. Hansen and P.-M. Poulain, "Quality control and interpolations of WOCE-TOGA drifter data," *J. Atmos. Ocean. Technol.*, vol. 13, no. 4, pp. 900–909, 1996.
[74] M. Berta, A. Griffa, T. M. Özgökmen, and A. C. Poje, "Submesoscale evolution of surface drifter triads in the Gulf of Mexico," *Geophys. Res. Lett.*, vol. 43, no. 22, pp. 12228–12233, 2016.
[75] K. Pearson, "Note on regression and inheritance in the case of two parents," *Proc. Roy. Soc. Lond.*, vol. 58, no. 347–352, pp. 240–242, 1895.
[76] A. Sentchev, P. Forget, and P. Fraunié, "Surface current dynamics under sea breeze conditions observed by simultaneous HF radar, ADCP and drifter measurements," *Ocean Dyn.*, vol. 67, no. 3–4, pp. 499–512, 2017.
[77] M. Berta *et al.*, "Estimating Lagrangian transport blending drifters with HF radar data and models: Results from the TOSCA experiment in the Ligurian Current (North Western Mediterranean Sea)," *Prog. Oceanogr.*, vol. 128, pp. 15–29, 2014.
[78] M. Berta *et al.*, "Improved surface velocity and trajectory estimates in the Gulf of Mexico from blended satellite altimetry and drifter data," *J. Atmos. Ocean. Technol.*, vol. 32, pp. 1880–1901, 2015.
[79] S. J. Orfanidis, *Optimum Signal Processing: An Introduction*, 2nd ed. Englewood Cliffs, NJ, USA: Prentice-Hall, 1996.

Lorenzo Paolo Corgnati received the M.S. degree in telecommunications engineering and the Ph.D. degree in electronic and communication engineering from Politecnico di Torino, Torino, Italy, in 2003 and 2007, respectively.

He is currently a Research Engineer at the Institute of Marine Sciences, National Research Council (CNR-ISMAR), La Spezia, Italy, where he is involved in sea surface currents monitoring using HF radars, interoperable and semantic-driven data management for oceanographic data, and 3-D reconstruction of sea surface, marine waves, underwater environment, and marine organisms detection using computer vision techniques. From 2001 to 2011, he was a Research Associate in the Remote Sensing Group, Politecnico di Torino, where he worked on atmospheric profiles using GPS signal in radio-occultation situation and fire risk forecasting and forest fires monitoring and early warning.

Carlo Mantovani received the M.S. degree in physics from the University of Parma, Parma, Italy, in 2001.

He is a Technical Scientist at the Consiglio Nazionale delle Ricerche, Institute of Marine Science (CNR-ISMAR), La Spezia, Italy, working mainly on technological development, and is currently in charge of the CNR-ISMAR HF radar infrastructure. He is involved in several national (RITMARE) and European projects (Jerico-Next, IMPACT, INCREASE, SeaDataCloud, etc.). He is a member of Eurogoos HF radar Task Team and participates to the coordination of the HF radar community at the national and European level.

Annalisa Griffa received the Ph.D. degree in oceanography from Scripps Institution of Oceanography, University of California San Diego, San Diego, CA, USA, in 1988.

She is a Senior Scientist at the Consiglio Nazionale delle Ricerche, Institute of Marine Science (CNR-ISMAR), La Spezia, Italy, and in charge of the RITMARE (Italian Flagship Project) Italian coastal HFR network. She is the author and coauthor of more than 80 peer-review publications and was a Principal Investigator in 30 European and U.S. projects on transport studies and prediction. She was an Advisor to 11 Ph.D. students and 8 post docs. Her research interests include transport and dispersion processes in the ocean using Lagrangian and HF radar data at different scales.

Maristella Berta received the M.S. degree in environmental physics from the University of Torino, Torino, Italy, in 2008 and the Ph.D. degree in environmental and industrial fluid mechanics from the University of Trieste, Trieste, Italy, in 2012, where she studied Lagrangian transport and connectivity through the FSLE technique.

In particular, she studies the current dynamics responsible for the dispersion of tracers, such as pollutant and larval transport. Her recent work focuses on passive transport driven by surface currents through the analysis of model outputs and observations.

Pierluigi Penna received the M.S. degree in computer science and the Ph.D. degree in information science and complex systems from the School of Science and Technology, University of Camerino, Camerino, Italy, in 2010 and 2014, respectively.

He has been a Specialized Technician in the Physical and Chemical Oceanography research group of the Consiglio Nazionale delle Ricerche, Institute of Marine Science, Ancona, Italy, since 1997. He is involved in physical and experimental oceanography, environmental monitoring programs, management of meteo-marine information systems, hardware and software development for the management of data acquisition systems, data processing, database, and interoperable and standardized access to data.

Paolo Celentano received the M.S. degree in science and technology of navigation from the Division Climate Science, University of Naples "Parthenope," Naples, Italy, in 2013. He is currently working toward the Ph.D. degree in applied sciences to the sea to the environment and the territory from the Division Sciences of the Sea of the Earth and Climate, University of Naples "Parthenope."

Since June 2016, he has been a Research Fellow at the Institute of Marine Sciences, National Research Council (CNR-ISMAR), involved in sea surface currents monitoring using acoustic current meters, multiparametric sensors, slocum glider, and yo–yo profiler. His research interests include physical and experimental oceanography, Lagrangian applications, and surface dynamics in coastal and open sea areas using drifting devices.

Lucio Bellomo was born in Palermo, Sicily, Italy, in 1983. He received the Ph.D. degree from the Laboratoire de Sondages Electromagnetiques de l'Environnement Terrestre (now part of the Mediterranean Institute of Oceanography), Toulon, France, in 2012, working on inverse scattering and time reversal.

He was an Associate Professor at the University of Toulon, Toulon, France, where he was involved in research on remote sensing of ocean currents and physical oceanography.

Daniel F. Carlson received the M.S. degree in physical oceanography from Florida State University, Tallahassee, FL, USA, in 2007 and the Ph.D. degree in physical oceanography from The Hebrew University of Jerusalem, Jerusalem, Israel, in 2014.

He was a Fulbright student at Weizmann Institute of Science from 2007 to 2008. He currently holds appointments with the Department of Earth, Ocean, and Atmospheric Science, Florida State University and the Arctic Research Centre, Aarhus University, Aarhus, Denmark. He is currently working on drone imaging systems to measure small scale (1–100 m) surface ocean dispersion and low-cost iceberg tracking beacons. His research focuses on near-surface Lagrangian transport in the ocean with applications to oil spills, marine debris, and ocean–glacier interactions.

Raffaele D'Adamo received the Graduate degree in biological sciences from the University of Naples Federico II, Napoli, Italy, in 1993.

Since 2001, he has been a Researcher at the Consiglio Nazionale delle Ricerche, Institute of Marine Science, Lesina, Italy. He is also involved in the development of the network of *in situ* monitoring system in the Mediterranean coastal area. He is a Marine Biologist with a vast experience of biological and environmental analyses. His research interests include coastal management and policy. His research activity deals with the interactions between biological communities and oceanographic variables for the management of the fishing activities. Moreover, his interest is focused on the development of early warning systems for the monitoring of high-weather events, such as storms and rains, to evaluate the effects of the runoff and the associated erosion resulting from intense rainfall that can represent a source of nutrient and pollutant loads from the land area.